$[Ru^{III}(L)O(H_2O)](ClO_4)_2 \cdot 2H_2O$, 123265-33-8; *trans*-$[Ru^{III}(L)O(H_2O)](ClO_4)_2$, 123265-32-7; *trans*-$[Ru^{VI}(L)(O)_2](ClO_4)_2$, 123265-35-0; benzyl alcohol, 100-51-6; isopropyl alcohol, 67-63-0; cyclohexene, 110-82-7; cyclooctene, 931-88-4; styrene, 100-42-5; norbornylene, 498-66-8; *cis*-stilbene, 645-49-8; *trans*-stilbene, 103-30-0; toluene, 108-88-3; adamantane, 281-23-2; ethylbenzene, 100-41-4; cumene, 98-82-8; tetrahydrofuran, 109-99-9; cyclobutanol, 2919-23-5; cyclohexanol, 108-93-0; benzaldehyde, 100-52-7; acetone, 67-64-1; cyclohexenone, 25512-62-3; cyclooctene oxide, 286-62-4; norbornylene oxide, 278-74-0; 1-adamantanol, 768-95-6; 2-adamantanol, 700-57-2; acetophenone, 98-86-2; *sec*-phenylethyl alcohol, 98-85-1; phenylisopropyl alcohol, 617-94-7; γ-butyrolactone, 96-48-0; cyclobutanone, 1191-95-3; cyclohexanone, 108-94-1; cyclohexen-1-ol, 4065-81-0; iodosylbenzene, 536-80-1.

Supplementary Material Available: Tables of anisotropic thermal parameters, hydrogen atomic parameters, bond distances and angles, least-squares planes, and experimental details for X-ray data collection (8 pages); listing of observed and calculated structure factors for $[Ru(C_{21}H_{28}N_2O_2)(O)(H_2O)](ClO_4)_2 \cdot 2H_2O$ (24 pages). Ordering information is given on any current masthead page.

Carbon Monoxide Cleavage by $(silox)_3Ta$ (silox = $^tBu_3SiO^-$): Physical, Theoretical, and Mechanistic Investigations

David R. Neithamer, Robert E. LaPointe, Ralph A. Wheeler, Darrin S. Richeson, Gregory D. Van Duyne, and Peter T. Wolczanski*,†

Contribution from the Department of Chemistry, Baker Laboratory, Cornell University, Ithaca, New York 14853. *Received March 10, 1989*

Abstract: Reduction of $(silox)_3TaCl_2$ (**1**, silox = $^tBu_3SiO^-$) with Na/Hg in THF leads to a three-coordinate, Ta(III) siloxide, $(silox)_3Ta$ (**2**). Derivatization of **2** with excess O_2 or H_2 provides $(silox)_3Ta{=}O$ (**3**) and $(silox)_3TaH_2$ (**4**), respectively. At 25 °C, carbonylation of **2** (0.1–1.0 atm) generates $^1/_2$**3** and $^1/_4[(silox)_3Ta]_2(\mu\text{-}C_2)$ (**5**), consistent with a CO uptake of 0.47 equiv. X-ray ($P\bar{1}$, R = 9.6%) structural, IR, and Raman studies of dicarbide **5** manifest a near-linear μ-C_2 bridge ($\angle$TaCC = 173 (3)°), a C=C double bond (1.37 (4) Å, ν(C=C) = 1617 cm^{-1}) and typical TaC double bonds (1.95 (2) Å, ν(Ta=C) = 709 cm^{-1}), respectively. EHMO calculations of a linear μ-C_2-bridged D_{3d} **5** indicate that the e_g^2 HOMO ($^3A_{2g}$, ^1E_g, $^1A_{1g}$) is ~80% Ta (d_{xz}, d_{yz}) and ~20% C (p_x, p_y). Magnetic susceptibility measurements of **5** from 2 to 300 K reveal a large temperature-independent susceptibility (25 °C, $\mu_{eff} = 1.93\mu_B$) and a singlet ground state, either ^1E_g, $^1A_{1g}$ (D_{3d}) or one arising from a Jahn–Teller distortion of the ^1E_g level. Treatment of **2** with CO (~1 atm) at −78 °C, followed by warming to 25 °C, results in an uptake of 0.97 equiv of CO and the production of an inseparable mixture of **3** and a monomeric ketenylidene, $(silox)_3Ta{=}C{=}C{=}O$ (**6**). Diamagnetic **6** (ν(C=O) = 2076 cm^{-1}, $^1J_{CC}$ = 100 Hz), a precursor to **5**, is linear according to EHMO calculations. Mechanistic investigations concerning formation of **5** and **6**, utilizing labeling experiments, kinetics, and chemical models, support the following sequence of reactions: (1) $(silox)_3Ta$ (**2**) binds CO to form unstable $(silox)_3TaCO$ (**2**-CO). (2) In donor solvents, **2**-CO is trapped and stabilized by the solvent (solvent = *S*) (−78 °C) as $(silox)_3STaCO$ (*S*-**2**-CO). (3) Aggregation of *S*-**2**-CO and equilibrium amounts of **2**-CO, dimerization of **2**-CO, or disproportionation of monocarbonyl species to $(silox)_3Ta(CO)_2$ (**2**-$(CO)_2$) and **2**, which quickly recombine, generates (−78 to −50 °C) red precipitate $[(silox)_3TaCO]_n$ ($[$**2**-CO$]_n$, n is probably 2). (4) In nondonor solvents **2**-CO either dimerizes or disproportionates to ultimately give $[$**2**-CO$]_n$. (5) Degradation of $[$**2**-CO$]_n$ (~5 °C), produces ketenylidene $(silox)_3Ta{=}C{=}C{=}O$ (**6**) and oxo $(silox)_3Ta{=}O$ (**3**). (6) Another $(silox)_3Ta$ (**2**) deoxygenates ketenylidene **6** (~0 °C), possibly via intermediate $(silox)_3Ta{=}C{=}\overline{C{-}O{-}Ta(silox)_3}$ (**6**·**2**), to afford oxo **3** and a transient vinylidene, $(silox)_3Ta{=}C{=}C$: (**2**-C_2), that electronically resembles CO, as substantiated by EHMO arguments. (7) A final $(silox)_3Ta$ (**2**) unit scavenges the vinylidene (**2**-C_2), resulting in $[(silox)_3Ta]_2(\mu\text{-}C_2)$ (**5**). Alternatives to the heterogeneous dissociative adsorption of CO, the first step in the Fischer–Tropsch process, are suggested on the basis of this work.

The Fischer–Tropsch (F–T) reaction,[1-4] the conversion of synthesis gas (CO/H_2) to hydrocarbons and oxygenates, has commanded the attention of the organometallic community for the past 10–15 years. During periods when olefin feedstocks are costly, the production of low molecular weight commodity chemicals from coal or natural gas via this method becomes economically attractive. The heterogeneously catalyzed F–T process is inherently nonselective since it produces a Schulz–Flory distribution of hydrocarbons, oxygenates, or both; thus homogeneous systems, considered to possess the advantage of greater selectivity, have attracted substantial interest. While a commercially feasible homogeneous F–T process has yet to be developed, some of the desired selectivity, especially toward methanol and C_2 oxygenates,[3] has been demonstrated. In addition, organometallic chemistry, through investigations of stoichiometric transformations involving carbon monoxide and dihydrogen, has dramatically increased our fundamental understanding of plausible individual steps that pertain to the F–T reaction.

The most widely accepted[4] mechanism for the heterogeneously catalyzed conversion of syngas to hydrocarbons consists of four critical steps: (1) carbon monoxide adsorbs ($(CO)_s$)[5] and dissociates on a metal surface, generating surface carbide (C_s) and oxide (O_s);[6-8] (2) surface hydrides formed upon chemisorption of di-

† Alfred P. Sloan Foundation Fellow (1987–1989).

(1) (a) Falbe, J. *Chemical Feedstocks from Coal*; John Wiley & Sons: New York, 1981. (b) Keim, W., Ed. *Catalysis in C_1 Chemistry*; D. Reidel: Dordrecht, The Netherlands, 1983. (c) Anderson, R. B. *The Fischer–Tropsch Synthesis*; Academic: New York, 1984. (d) Anderson, J. R.; Boudart, M. *Catalysis*; Springer-Verlag: Berlin, 1981; Vol. 1.

(2) (a) Biloen, P.; Sachtler, W. M. H. *Adv. Catal.* **1981**, *30*, 165–216. (b) Bell, A. T. *Catal. Rev.—Sci. Eng.* **1981**, *23*, 203–232. (c) Rofer-DePoorter, C. K. *Chem. Rev.* **1981**, *81*, 447–474. (d) Masters, C. *Adv. Organomet. Chem.* **1979**, *17*, 61–103. (e) Vannice, M. A. *Catal. Rev.—Sci. Eng.* **1976**, *14*, 153–191.

(3) Dombek, B. D. *Adv. Catal.* **1983**, *32*, 325–416.

(4) (a) Fischer, F.; Tropsch, H. *Chem. Ber.* **1926**, *59*, 830–836. (b) Craxford, S. R.; Rideal, E. K. *J. Chem. Soc.* **1939**, 1604–1614.

(5) Sung, S.-S.; Hoffmann, R. *J. Am. Chem. Soc.* **1985**, *107*, 578–854, and references therein.

(6) (a) Low, G. G.; Bell, A. T. *J. Catal.* **1979**, *57*, 397–405. (b) Roberts, M. W. *Chem. Soc. Rev.* **1977**, *6*, 373–391. (c) Brodén, G.; Rhodin, T. N.; Brucker, C.; Benbow, R.; Hurych, Z. *Surf. Sci.* **1976**, *59*, 593–611.

0002-7863/89/1511-9056$01.50/0

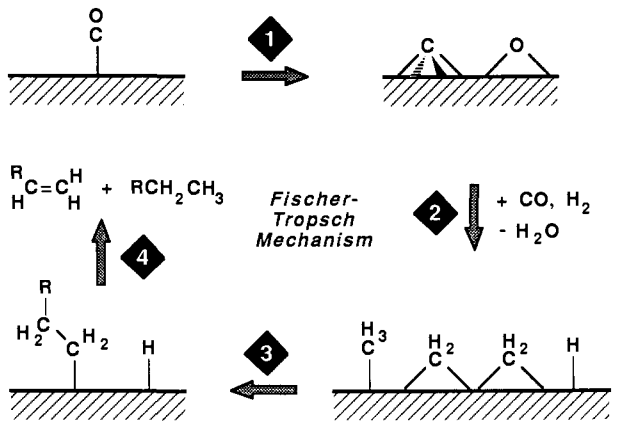

hydrogen transfer to the C_s, producing methylene ($(CH_2)_s$) and methyl ($(CH_3)_s$) fragments,[9-11] and to the O_s, forming water;[12] (3) the growth of alkyl ($(CH_2R)_s$) chains occurs through oligomerization of $(CH_2)_s$ units;[9-12] (4) reductive elimination of a surface alkyl and hydride or β-elimination from $(CH_2CH_2R)_s$ causes the release of a product alkane or olefin, respectively, upon desorption.[13] This sequence of transformations is essentially the same as that postulated by Fischer and Tropsch in 1926, with minor modifications.[4] Various organometallic species have been shown to model each individual step,[14] and a recent reaction sequence involving carbonylation of $[(silox)_2TaH_2]_2$[15] (silox = $^tBu_3SiO^-$)[16,17] demonstrated the deoxygenation of CO in conjunction with the formation of C–H and C–C bonds.

The initial step in the overall process, the dissociative adsorption of CO, has been modeled by late metal carbonyl cluster carbides.[7,8] Formation of these intriguing complexes is often accompanied by the release of CO_2 ($2CO \rightarrow C + CO_2$), suggesting that two $(CO)_s$ can combine to generate surface carbide, rather than $(CO)_s$ dissociation, followed by O_s abstraction by CO or $(CO)_s$ to give CO_2. One of the most interesting examples of homogeneous CO dissociation has been observed by Shriver et al.,[8] who were able to follow the breakdown of a CO in $Fe_4(CO)_{13}^{2-}$ upon addition of a Lewis acid; treatment of a resulting II-CO complex with H^+ led to the formation of a tetrairon butterfly carbide with loss of H_2O, and eventually to the production of methane. In homogeneous systems, the cleavage of a carbon–oxygen bond derived from CO usually occurs following alkyl[18] or hydride migration.[19] Scission of the C–O bond in the resultant aldehyde or ketone produces a hydrocarbyl fragment and an oxide.[20] Mayer and co-workers have reported numerous scissions of heterocumulenes[21] and an intriguing addition of cyclopentanone to $WCl_2(PMePh_2)_4$ that ultimately leads to $W(=O)(=\overline{C(CH_2)_3CH_2})Cl_2(PMePh_2)_2$.[22] These systems all contain early transition metals, which form strong metal–oxygen bonds, thereby providing a thermodynamic bias for the bond-breaking process.

Early metal carbides are less prevalent than the aforementioned late metal cluster species. Alcoholysis of $W_2(NMe_2)_6$ yielded an isopropoxide-based tetratungsten butterfly carbide in which the W_4C unit was created through decomposition of a dimethylamido ligand.[23] Related dicarbides have been synthesized through procedures utilizing acetylides[24] and alkyne metatheses.[25] The breakdown of carbon monoxide has resulted in carbides or complexes in which the carbon and oxygen originating from CO are distinctly separated. In a study reminescent of carbonyl clusters, Chisholm et al. observed the formation of a tungsten butterfly carbide, $W_4(C)(O)(O^iPr)_{12}$, when carbonyl-bridged $W_4(\mu\text{-}CO)_2(O^iPr)_{12}$ was treated with $W_2(O^tBu)_6$ in ^iPrOH/hexane.[26] In this instance, the coordinatively unsaturated $(W{\equiv}W)^{6+}$ unit acts as a Lewis acid to break up the tetramer and then serves as a reductant to cleave the CO. A related investigation revealed that $(\eta^5\text{-}C_5Me_5)_2Sm(THF)_2$, a powerful one-electron reductant, could reductively homologate CO, generating a ketenecarboxylate ligand.[27]

In a 1986 communication,[28] $(silox)_3Ta$ was reported to cleave carbon monoxide, providing an oxo complex, $(silox)_3Ta{=}O$, and a dicarbide, $[(silox)_3Ta]_2(\mu\text{-}C_2)$.[29] Three-coordinate $(silox)_3Ta$ attacks CO in a bifunctional manner, both as a potent reductant (Ta(III), d^2) and as a coordinatively unsaturated, oxophilic metal

(7) (a) Horowitz, C. P.; Shriver, D. F. *Adv. Organomet. Chem.* **1984**, *23*, 219–305. (b) Bradley, J. S. *Adv. Organomet. Chem.* **1983**, *22*, 1–58. (c) Muetterties, E. L.; Stein, J. *Chem. Rev.* **1979**, *79*, 479–490. (d) Tachikawa, M.; Muetterties, E. L. *Prog. Inorg. Chem.* **1981**, *28*, 203–238.

(8) (a) Shriver, D. F.; Sailor, M. J. *Acc. Chem. Res.* **1988**, *21*, 374–379. (b) Horwitz, C. P.; Shriver, D. F. *J. Am. Chem. Soc.* **1985**, *107*, 8147–8153.

(9) (a) Biloen, P.; Helle, J. N.; van den Berg, F. G. A.; Sachtler, W. M. H. *J. Catal.* **1983**, *81*, 450–463. (b) Biloen, P.; Helle, J. N.; Sachtler, W. M. H. *Ibid.* **1979**, *58*, 95–107. (c) Araki, M.; Ponec, V. *Ibid.* **1976**, *44*, 439–448. (d) Zhang, X.; Biloen, P. *Ibid.* **1986**, *98*, 468–476. (e) Biloen, P. *Recl. Trav. Chim. Pays-Bas* **1980**, *99*, 33–38. (f) Vannice, M. A.; Sudhaker, C. *J. Phys. Chem.* **1984**, *88*, 2429–2432. (g) Mims, C. A.; McCandlish, L. E. *Ibid.* **1987**, *91*, 929–937.

(10) (a) Brady, R. C., III; Pettit, R. *J. Am. Chem. Soc.* **1981**, *103*, 1287–1289. (b) Brady, R. C., III; Pettit, R. *J. Am. Chem. Soc.* **1980**, *102*, 6182–6184.

(11) (a) George, P. M.; Avery, N. R.; Weinberg, W. H.; Tebbe, F. N. *J. Am. Chem. Soc.* **1983**, *105*, 1393–1394. (b) Erley, W.; McBreen, P. H.; Ibach, H. *J. Catal.* **1983**, *84*, 229–234. (c) Barteau, M. A.; Feulner, P.; Stengl, R.; Broughton, J. Q.; Menzel, D. *Ibid.* **1985**, *94*, 51–59. (d) Kaminsky, M. P.; Winograd, N.; Geoffroy, G. L. *J. Am. Chem. Soc.* **1986**, *108*, 1315–1316. (e) Lee, M. B.; Yang, Q. Y.; Tang, S. L.; Ceyer, S. T. *J. Chem. Phys.* **1986**, *85*, 1693–1694.

(12) Ekstrom, A.; Lapszewicz, J. *J. Phys. Chem.* **1984**, *88*, 4577–4580.

(13) Zheng, C.; Apeloig, Y.; Hoffmann, R. *J. Am. Chem. Soc.* **1988**, *110*, 749–774.

(14) (a) Herrmann, W. A. *Adv. Organomet. Chem.* **1982**, *20*, 159–263. (b) Herrmann, W. A. *Angew. Chem., Int. Ed. Engl.* **1982**, *21*, 117–130. (c) Isobe, K.; Vázquez de Miguel, A.; Bailey, P. M.; Okeya, S.; Maitlis, P. M. *J. Chem. Soc., Dalton Trans.* **1983**, 1441–1447. (d) Saez, I. M.; Meanwell, N. J.; Nutton, A.; Isobe, K.; Vázquez de Miguel, A.; Bruce, D. W.; Okeya, S.; Andrews, D. G.; Ashton, P. R.; Johnstone, I. R.; Maitlis, P. M. *Ibid.* **1986**, 1565–1575. (e) Saez, I. M.; Andrews, D. G.; Maitlis, P. M. *Polyhedron* **1988**, *7*, 827–835. (f) Gladysz, J. A. *Adv. Organomet. Chem.* **1982**, *20*, 1–38. (g) Wolczanski, P. T.; Bercaw, J. E. *Acc. Chem. Res.* **1980**, *13*, 121–127.

(15) (a) Toreki, R.; LaPointe, R. E.; Wolczanski, P. T. *J. Am. Chem. Soc.* **1987**, *109*, 7558–7560. (b) LaPointe, R. E.; Wolczanski, P. T. *J. Am. Chem. Soc.* **1986**, *108*, 3535–3537.

(16) LaPointe, R. E.; Wolczanski, P. T.; Van Duyne, G. D. *Organometallics* **1985**, *4*, 1810–1818.

(17) (a) Weidenbruch, M.; Pierrard, C.; Pesel, H. *Z. Naturforsch., B: Anorg. Chem. Org. Chem.* **1978**, *33B*, 1468–1471. (b) Dexheimer, E. M.; Spialter, L.; Smithson, L. D. *J. Organomet. Chem.* **1975**, *102*, 21–27.

(18) (a) Marsella, J. A.; Huffman, J. C.; Folting, K.; Caulton, K. G. *Inorg. Chem. Acta* **1985**, *96*, 161–170. (b) Marsella, J. A.; Huffman, J. C.; Folting, K.; Caulton, K. G. *J. Am. Chem. Soc.* **1981**, *103*, 5596–5598. (c) Wood, C. D.; Schrock, R. R. *Ibid.* **1979**, *101*, 5421–5422. (d) Planalp, R. P.; Andersen, R. A. *Ibid.* **1983**, *105*, 7774–7775. (e) Blenkers, J.; de Liefde Meijer, H. J.; Teuben, J. H. *Organometallics* **1983**, *2*, 1483–1484. (f) Shapley, J. R.; Park, J. T.; Churchill, M. R.; Ziller, J. W.; Beanan, L. R. *J. Am. Chem. Soc.* **1984**, *106*, 1144–1145. (g) Jacobsen, E. N.; Trost, M. K.; Bergman, R. G. *Ibid.* **1986**, *108*, 8092–8094.

(19) (a) Erker, G. *Acc. Chem. Res.* **1984**, *17*, 103–109. (b) Kropp, K.; Skibbe, V.; Erker, G.; Krüger, C. *J. Am. Chem. Soc.* **1983**, *105*, 3353–3354. (c) Erker, G.; Kropp, K.; Krüger, C.; Chiang, A.-P. *Chem. Ber.* **1982**, *115*, 2447–2640.

(20) (a) Erker, G.; Dorf, U.; Atwood, J. L.; Hunter, W. E. *J. Am. Chem. Soc.* **1986**, *108*, 2251–2257. (b) Erker, G.; Schlund, R.; Albrecht, M.; Sarter, C. *J. Organomet. Chem.* **1988**, *353*, C24–C29.

(21) Bryan, J. C.; Geib, S. J.; Rheingold, A. L.; Mayer, J. M. *J. Am. Chem. Soc.* **1987**, *109*, 2826–2828.

(22) Bryan, J. C.; Mayer, J. M. *J. Am. Chem. Soc.* **1987**, *109*, 7213–7214.

(23) Chisholm, M. H.; Folting, K.; Huffman, J. C.; Leonelli, J.; Marchant, N. S.; Smith, C. A.; Taylor, L. C. E. *J. Am. Chem. Soc.* **1985**, *107*, 3722–3724.

(24) (a) Blau, R. J.; Chisholm, M. H.; Folting, K.; Wang, R. J. *J. Chem. Soc., Chem. Commun.* **1985**, 1582–1585. (b) Ogawa, H.; Joh, T.; Takahashi, S.; Sonogashira, K. *Ibid.* **1985**, 1220–1221.

(25) Listemann, M. L.; Schrock, R. R. *Organometallics* **1985**, *4*, 75–83.

(26) (a) Chisholm, M. H.; Clark, D. L.; Huffman, J. C.; Smith, C. A. *Organometallics* **1987**, *6*, 1280–1291. (b) Chisholm, M. H.; Heppert, J. A.; Huffman, J. C.; Streib, W. E. *J. Chem. Soc., Chem. Commun.* **1985**, 1771–1773.

(27) Evans, W. J.; Grate, J. W.; Hughes, L. A.; Zhang, H.; Atwood, J. L. *J. Am. Chem. Soc.* **1985**, *107*, 3728–3730.

(28) LaPointe, R. E.; Wolczanski, P. T.; Mitchell, J. F. *J. Am. Chem. Soc.* **1986**, *108*, 6382–6384.

(29) For related late metal dicarbon-containing species, see: (a) Brice, M. D.; Penfold, B. R. *Inorg. Chem.* **1972**, *11*, 1381–1384. (b) Dellaca, R. J.; Penfold, B. R.; Robinson, B. H.; Robinson, W. T.; Spencer, J. L. *Ibid.* **1970**, *9*, 2204–2211. (c) Goldberg, S. Z.; Duesler, E. N.; Raymond, K. N. *Ibid.* **1972**, *11*, 1397–1401.

center. It is the latter function that separates this highly reactive complex from species that couple carbonyl units.[30-32] A mechanistic investigation of the ditantalum dicarbide formation is provided herein, along with pertinent synthetic, theoretical, and physical studies of the complex and its precursors.

Synthetic and Spectroscopic Studies

(silox)$_3$Ta (2). Treatment of $TaCl_5$ with 3.0 equiv of Na(silox) in toluene at 25 °C for 9 h followed by 15 h at reflux afforded colorless (silox)$_3$TaCl$_2$ (**1**)[15,17] in 80% yield after crystallization from hexanes (eq 1). As has been observed for other silox

$$TaCl_5 + 3Na(silox) \xrightarrow[-3NaCl]{toluene} \underset{\mathbf{1}}{(silox)_3TaCl_2} \quad (1)$$

halides/oxides,[16,17] dichloride **1** is extremely robust, melting at ~270 °C. The complex is also relatively air-stable and hydrolyzes slowly in moist air. The reduction of **1** to (silox)$_3$Ta (**2**) was accomplished with 0.9% Na/Hg (4.0 equiv of Na) in THF (eq 2). During the course of warming from −78 to 25 °C and stirring

$$\underset{\mathbf{1}}{(silox)_3TaCl_2} \xrightarrow[THF,\ 25\ °C,\ 2\ h]{Na/Hg,\ -2NaCl} \underset{\mathbf{2}}{(silox)_3Ta} \quad (2)$$

for 2 h, the THF solution changed from colorless to purple, then to blue, and finally to blue-green. The THF was removed and hexane added; concentration of the filtrate and cooling to −78 °C resulted in light blue crystals of **2** (74%). A cryoscopic molecular weight determination in benzene was consistent with a monomeric formulation (calcd, 827; found, 800). Magnetic susceptibility measurements from 2 to 300 K (Faraday balance) and sharp resonances in the ^{1}H (δ 1.32), ^{13}C (δ 22.83 (SiC), 31.75 (Me)), and ^{29}Si (δ 18.63) NMR spectra indicated that the Ta(III), d^2 complex is diamagnetic. A sterically favorable trigonal (D_{3h}) arrangement of the silox groups is consistent with a singlet ground state ($^1A_1'$), provided both electrons occupy the d_{z^2} orbital ($a_1'^2$).[33] Extended Hückel calculations performed on hypothetical (HO)$_3$Ta indicated that D_{3h} symmetry is preferred over pyramidal (C_{3v}) or T-shaped (C_{2v}) structures.

Derivatization of (silox)$_3$Ta (**2**) was accomplished via the addition of oxygen and through hydrogenation. Exposure of (silox)$_3$Ta (**2**) to 1 atm of dioxygen in benzene solution at 25 °C resulted in rapid dissipation of the blue color (eq 3). Crystal-

$$\underset{\mathbf{2}}{(silox)_3Ta} \xrightarrow[benzene,\ 25\ °C]{O_2\ (1\ atm)} \underset{\mathbf{3}}{(silox)_3Ta{=}O} \quad (3)$$

lization from Et_2O provided off-white crystals of (silox)$_3$Ta=O (**3**; 43%), characterized by a Ta=O stretch at 905 cm^{-1} in its IR spectrum, indicative of a terminal oxo.[34,35] Blue solutions of **2** bleach within 1 h upon treatment with 1 atm of dihydrogen, affording (silox)$_3$TaH$_2$ (**4**) as colorless crystals in ~80% yield (eq 4).[15] Dihydride **4** exhibited a typical downfield ^{1}H NMR

$$\underset{\mathbf{2}}{(silox)_3Ta} \xrightarrow[benzene,\ 25\ °C]{H_2\ (1\ atm)} \underset{\mathbf{4}}{(silox)_3TaH_2} \quad (4)$$

shift (δ 21.99) corresponding to the TaH_2 unit and two strong IR bands at 1725 (1250) and 750 (570) cm^{-1} assigned as the Ta–H(D)$_2$ stretch and scissoring modes, respectively. In view of the latter absorption and the steric requirements of the silox ligands, **4** probably possesses a trigonal-bipyramidal (D_{3h}) geometry.

CO Cleavage. When a benzene solution of (silox)$_3$Ta (**2**) at 25 °C was treated with 1.00 equiv of carbon monoxide (~100 Torr), the blue color immediately discharged concomitant with an uptake of 0.47 equiv of CO and formation of a red precipitate.[28] Filtration of a hexane slurry resulted in a brick-red solid, identified as [(silox)$_3$Ta]$_2$(μ-C$_2$) (**5**; 46% based on Ta), and a pink solution; removal of hexane from the latter yielded an off-white solid containing crude (silox)$_3$Ta=O (**3**; 47%, eq 5). Spectral com-

$$\underset{\mathbf{2}}{(silox)_3Ta} + \tfrac{1}{2}CO \xrightarrow[benzene]{25\ °C} \tfrac{1}{2}\underset{\mathbf{3}}{(silox)_3Ta{=}O} + \tfrac{1}{4}\underset{\mathbf{5}}{[(silox)_3Ta]_2(\mu\text{-}C_2)} \quad (5)$$

parisons and a mixed melting point test (320 °C) verified that the oxo (**3**) obtained from CO scission and purified via sublimation was identical with that generated in the oxygenation of **2** (eq 3). Crystallization of the red solid from hot THF produced analytically pure dicarbide **5**.

The initial assignment of **5** as a dimer rather than alternative [(silox)$_3$TaC]$_n$ species was based on a series of isotopic labeling experiments. Infrared spectra of **5** derived from either CO or C^{18}O exhibited a band at 709 cm^{-1} in addition to absorptions readily attributable to silox. The IR spectrum of the oxo (**3**) produced in the C^{18}O experiment revealed a shift from 905 cm^{-1} to a region (ν(Ta=^{18}O)$_{calcd}$ = 858 cm^{-1}) where it was obscured by the broad manifold of Si–O, Si–C, and ^{t}Bu absorptions (800–900 cm^{-1}) characteristic of silox-containing complexes. When ^{13}CO was the substrate, the critical band of **5** shifted to 682 cm^{-1}. Furthermore, exposure of (silox)$_3$Ta (**2**) to a 1:1 mixture of CO to ^{13}CO provided a sample of **5** that displayed bands at 709, 695, and 682 cm^{-1} in an approximate 1:2:1 ratio, indicative of a two-carbon bridge. This IR band may be assigned as either a Ta=C stretching or TaCCTa rocking vibration, but the former appears more realistic energetically.

NMR spectra of the dicarbide (**5**) were also revealing. Whereas the oxo (**3**) manifested typical ^{13}C resonances in C_6D_6 at δ 23.71 (SiC) and δ 30.54 (Me) and a silox singlet in the ^{1}H NMR at δ 1.27 (1.23 in THF-d_8), resonances of the dicarbide were broadened ($\nu_{1/2}$ ~ 10 Hz) and shifted substantially from the normal region for diamagnetic silox complexes. In the ^{1}H NMR (C_6D_6) spectrum, the silox protons resonated at δ 2.03 (1.88 in THF-d_8) while the SiC (δ 53.45) and Me (δ 44.50) carbons reversed positions and shifted downfield in the ^{13}C (THF-d_8, 40 °C) spectrum. The aforementioned broadness of the resonances might be attributed to the low solubility of **5** and corresponding sample heterogeneity, but the positional changes are indicative of paramagnetic character. The magnitudes of the deviations from typical diamagnetic chemical shifts thus appear to be inversely proportional to the distance between specific sites and the μ-C$_2$ bridge. Even when [(silox)$_3$Ta]$_2$(μ-^{13}C$_2$) (**5**-^{13}C$_2$) was examined, the dicarbide unit could not be located.

Chemical characterization provided further evidence for the existence of the dicarbide bridge in **5**. Hydrolysis of [(silox)$_3$Ta]$_2$(μ-C$_2$) (**5**) in THF-d_8 over a period of 15 h at 110 °C gave ethylene and (silox)H as the only NMR-observable products; presumably, hydrated Ta_2O_5 is also generated (eq 6). An attempt

$$\underset{\mathbf{5}}{[(silox)_3Ta]_2(\mu\text{-}C_2)} \xrightarrow[THF\text{-}d_8,\ 110\ °C,\ 15\ h]{H_2O\ (excess)} C_2H_4 + 6(silox)H + Ta_2O_5 \quad (6)$$

to produce C_2H_4 and (silox)$_3$Ta=O (**3**) through stoichiometric cleavage of the bridge with 2.0 equiv of H_2O resulted in an incomplete reaction and (silox)H formation. The relatively drastic conditions of these hydrolyses suggest that penetration of the hydrocarbon periphery of **5** by a polar reagent such as water must be extremely difficult. Severing M–C bonds of early transition metals with electrophilic reagents (e.g., H^+ sources) usually occurs rapidly.[36] Furthermore, hydrolyses of Ta–OSi linkages must occur

(30) Kahn, B. E.; Rieke, R. D. *Chem. Rev.* **1988**, *88*, 733–745.
(31) Berry, D. H.; Bercaw, J. E.; Jircitano, A. J.; Mertes, K. B. *J. Am. Chem. Soc.* **1982**, *104*, 4712–4715.
(32) (a) Bianconi, P. A.; Vrtis, R. N.; Rao, C. P.; Williams, I. D.; Engeler, M. P.; Lippard, S. J. *Organometallics* **1987**, *6*, 1968–1977. (b) Bianconi, P. A.; Williams, I. D.; Engeler, M. P.; Lippard, S. J. *J. Am. Chem. Soc.* **1986**, *108*, 311–313. (c) Vrtis, R. N.; Rao, C. P.; Bott, S. G.; Lippard, S. J. *Ibid.* **1988**, *110*, 7564–7566.
(33) (a) Alyea, E. C.; Bradley, D. C.; Copperthwaite, R. G.; Sales, K. D. *J. Chem. Soc., Dalton Trans.* **1973**, 185–191. (b) Wood, J. S. *Inorg. Chem.* **1968**, *7*, 852–859.
(34) Nugent, W. A.; Mayer, J. M. *Metal–Ligand Multiple Bonds*; John Wiley & Sons: New York, 1988.
(35) According to IR criteria posed by Bercaw et al., (silox)$_3$Ta=O (**3**) is intermediate between a class a (ν(M≡O) ≈ 930–1000 cm^{-1}) and class b (ν(M=O) < 930 cm^{-1}) oxo complex. (a) Parkin, G.; Bercaw, J. E. *J. Am. Chem. Soc.* **1989**, *111*, 391–393. (b) van Asselt, A.; Burger, B. J.; Gibson, V. C.; Bercaw, J. E. *J. Am. Chem. Soc.* **1986**, *108*, 5347–5349.
(36) For an exception, see: Feinstein-Jaffe, I.; Gibson, D.; Lippard, S. J.; Schrock, R. R.; Spool, A. *J. Am. Chem. Soc.* **1984**, *106*, 6305–6310.

at least as fast as bridge cleavage, presumably due to the kinetic accessibility of the O lone pairs to protolysis.[37]

In anticipation of discovering an oxidative degradation pathway that would cleanly yield CO for mechanistic labeling experiments, $[(silox)_3Ta]_2(\mu\text{-}C_2)$ (**5**) was exposed to excess dioxygen (eq 7).

$$\underset{\mathbf{5}}{[(silox)_3Ta]_2(\mu\text{-}C_2)} \xrightarrow[\text{pentane, 25 °C}]{O_2\ (1\ atm),\ 30\ min} \underset{\mathbf{3}}{(silox)_3Ta{=}O} + \underset{\mathbf{6}}{(silox)_3Ta{=}C{=}C{=}O} + \ldots \quad (7)$$

While the expected $(silox)_3Ta{=}O$ (**3**) was produced, the C_2 linkage remained intact over a period of 30 min, becoming incorporated into a monomeric ketenylidene complex, $(silox)_3Ta{=}C{=}C{=}O$ (**6**). Examination of the oxygenation reaction by ^1H NMR showed that ~45% of the oxo (**3**) and ~40% of the ketenylidene (**6**) were generated in addition to several unidentified decomposition products. Although the desired degradation did not occur, this experiment does underscore the kinetic stability of the Ta=C and C=C fragments.

Low-temperature carbonylation (>100 Torr) of $(silox)_3Ta$ (**2**) resulted in a diminution of dicarbide (**5**) relative to a different CO cleavage product, ketenylidene $(silox)_3Ta{=}C{=}C{=}O$ (**6**). Treatment of **2** in toluene at −78 °C with 305 Torr CO (10.0 equiv) yielded, upon warming to 25 °C (1.5 h), an approximately equimolar mixture of $(silox)_3Ta{=}O$ (**3**) and $(silox)_3Ta{=}C{=}C{=}O$ (**6**), concomitant with an uptake of 0.91 equiv of carbon monoxide, implicating the stoichiometry in eq 8. Unfortunately,

$$\underset{\mathbf{2}}{(silox)_3Ta} + CO \xrightarrow[-78 \rightarrow 25\ °C]{\text{toluene}} \tfrac{1}{2}\underset{\mathbf{3}}{(silox)_3Ta{=}O} + \tfrac{1}{2}\underset{\mathbf{6}}{(silox)_3Ta{=}C{=}C{=}O} \quad (8)$$

all efforts directed toward the separation of **6** from the oxo (**3**) have been unsuccessful. An independent evaluation of the reactivity of $(silox)_3Ta{=}O$ (**3**) suggested that this complex is virtually inert; hence, *in each mechanistic experiment described in the text, oxo **3** is treated as a present but noninteractive partner to ketenylidene **6***. Color changes and the formation and dissolution of precipitates observed during the course of ketenylidene (**6**) formation were indicative of the complexity of this reaction. Initial exposure of **2** to CO at −78 °C resulted in the immediate fading of the blue color and precipitation of a red solid. As the solution was permitted to warm to 25 °C, the red precipitate dissolved (~5–10 °C) with loss of color to yield a pale orange solution. Upon filtration in hexane and removal of the solvent, the mixture of **3** and **6** was obtained.

Identification of the ketenylidene[38-42] was confirmed through various NMR and IR spectra of isotopically labeled derivatives. The ^{13}C NMR spectrum of $(silox)_3Ta{=}^{13}C{=}^{13}C{=}O$ (**6**-$^{13}C_2$) revealed two doublets ($^1J_{CC}$ = 100 Hz) at δ 135.96 (Ta*C*CO) and δ 142.51 (TaC*C*O), which accompanied the silox resonances (δ 23.64 (SiC), 30.42 (Me)) of this diamagnetic complex. The carbon bound to Ta (C_α) was broadened due to interaction with the quadrupolar nucleus of the heavy metal.[43] The 100 Hz coupling constant is reasonable for a linkage of two sp centers,

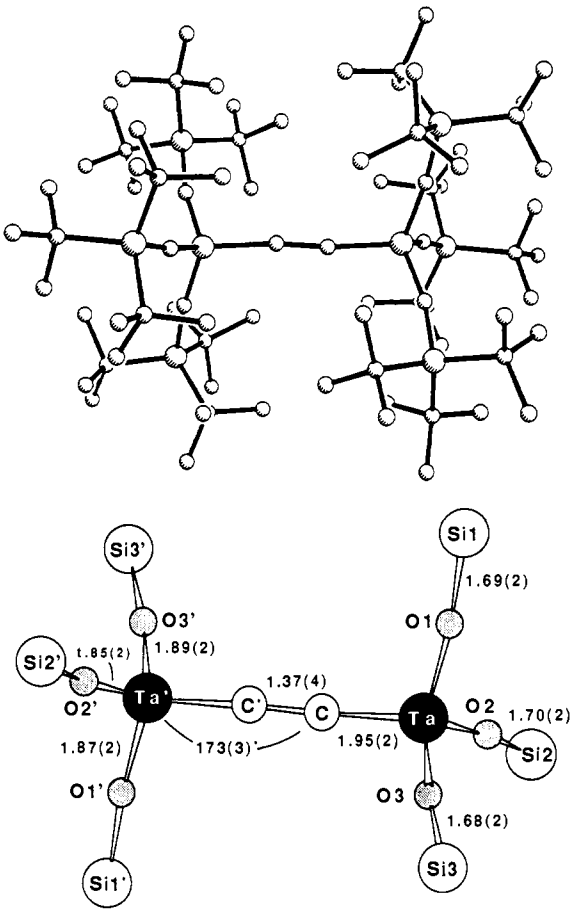

Figure 1. Molecular structure and skeletal view of $[(silox)_3Ta]_2(\mu\text{-}C_2)$ (**5**). Bond distances are in angstroms. Average bond angles: O–Ta–O, 110 (4)°; C–Ta–O, 109 (3)°; Ta–O–Si, 171 (2)°.

although a paucity of comparable monomeric complexes is evident. Related μ_3-ketenylidene ligands of trimetallic clusters possess C–C coupling constants in the 74–96 Hz range.[41] A strong infrared band observed at 2076 cm^{-1} for **6** can be assigned to the C=O stretch, since it shifts to 2011 cm^{-1} for **6**-$^{13}C_2$. From a 1:1 mixture of CO and ^{13}CO, the IR spectrum of the resulting ketenylidene exhibited four approximately equally intense bands at 2076, 2065, 2022, and 2011 cm^{-1}, indicative of a statistical mixture of **6**, $(silox)_3Ta{=}^{13}C{=}C{=}O$ (**6**-^{13}CC), $(silox)_3Ta{=}C{=}^{13}C{=}O$ (**6**-C^{13}C), and **6**-$^{13}C_2$, respectively. Strong coupling between the C=O and C=C linkages is evident, yet the locations of other vibrations associated with the ketenylidene ligand[44] have thus far escaped verification.

Physical and Theoretical Studies

$[(silox)_3Ta]_2(\mu\text{-}C_2)$ (5). A single-crystal X-ray structure determination (Cu Kα, triclinic, $P\bar{1}$) of $[(silox)_3Ta]_2(\mu\text{-}C_2)$ (**5**) confirmed the two-carbon bridge. As the structure refinement proceeded, it became clear that the peripheral ^{t}Bu groups were severely disordered. The best disorder model proved to be one in which a particular silox (Si1) contained two different types of ^{t}Bu groups. Constraints were applied to the geometries of each ^{t}Bu fragment on the remaining silox ligands. The final structure model reflects these problems, as judged by the *R* of 0.096 and the large standard deviations ascribed to the distances and angles. Although the periphery of the molecule had to be refined isotropically, the core of the dicarbide (Ta, Si, O, μ-C) was treated anisotropically and was unaffected by the various disorder models. As Figure 1 shows, virtual D_{3d} symmetry is manifested for **5**, with

(37) Hillhouse, G. L.; Bercaw, J. E. *J. Am. Chem. Soc.* **1984**, *106*, 5472–5478.

(38) Seyferth, D.; Hallgren, J. E.; Eschbach, C. S. *J. Am. Chem. Soc.* **1974**, *96*, 1730–1737.

(39) (a) Holmgren, J. S.; Shapley, J. R. *Organometallics* **1984**, *3*, 1322–1323. (b) Hriljac, J. A.; Shriver, D. F. *J. Am. Chem. Soc.* **1987**, *109*, 6010–6015, and references therein.

(40) Sailor, J. M.; Brock, C. P.; Shriver, D. F. *J. Am. Chem. Soc.* **1987**, *109*, 6015–6022. This paper includes a brief molecular orbital treatment of $[Ru_3(CO)_6(\mu\text{-}CO)_3(\mu_3\text{-}CCO)]^{2-}$.

(41) Went, M. J.; Sailor, M. J.; Bogdan, P. L.; Brock, C. P.; Shriver, D. F. *J. Am. Chem. Soc.* **1987**, *109*, 6023–6029. This paper includes MO treatments of $[M_3(CO)_9(\mu_3\text{-}CCO)]^{2-}$ (M = Fe, Ru, Os) and J_{CC} values for $M_3(\mu_3\text{-}CCO)$ complexes.

(42) For a report of an apparent monomeric ketenylidene transient, see: List, A. K.; Hillhouse, G. L.; Rheingold, A. L. *J. Am. Chem. Soc.* **1988**, *110*, 4855–4856.

(43) Brevard, C.; Granger, P. *Handbook of High Resolution Multinuclear NMR*; John Wiley & Sons: New York, 1981.

(44) For a discussion of the vibrational spectroscopy of $M_3(\mu_3\text{-}CCO)$ complexes and the possible occurrence of the ketenylidene ligand on metal surfaces, see: Sailor, M. J.; Shriver, D. F. *J. Am. Chem. Soc.* **1987**, *109*, 5039–5041.

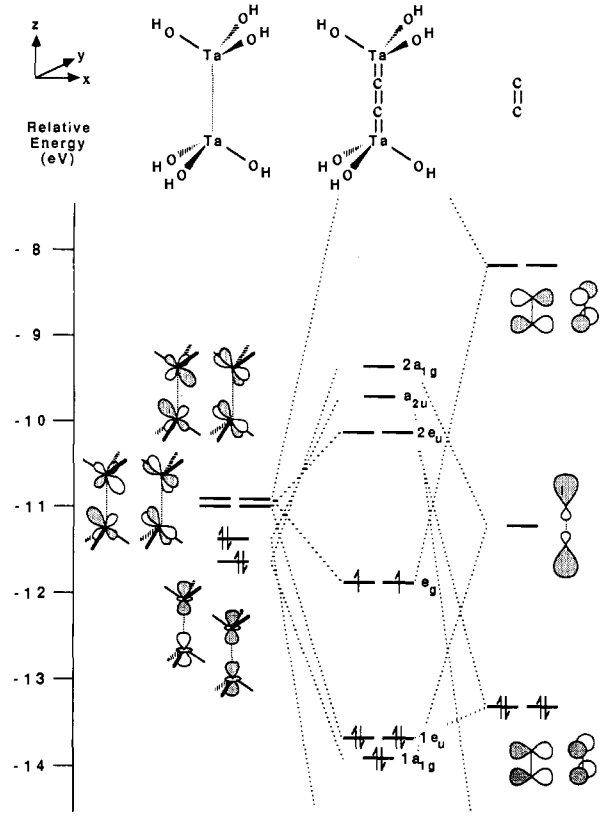

Figure 2. Truncated molecular orbital diagram of $[(HO)_3Ta]_2(\mu\text{-}C_2)$ (**5′**), a model of $[(silox)_3Ta]_2(\mu\text{-}C_2)$ (**5**).

the center of inversion located at the midpoint of the μ-C_2 unit. The geometry about the tantalum center is best described as pseudo-T_d with the O–Ta–O and O–Ta–C angles averaging 110 (4) and 109 (3)°, respectively. The bridge is within 3σ of being linear, as indicated by the Ta–C1–C1′ angle of 173 (3)°. The C1–C1′ bond length, 1.37 (4) Å, is close to that of a typical double bond (1.34 Å) while the 1.95 (2) Å Ta–C1 distance falls in the range of tantalum alkylidenes (1.89–2.07 Å).[45] Care must be taken not to place much emphasis on these distances because of their large standard deviations. While the bridging mode of the dicarbide was confirmed, the ambiguity regarding the degree of linearity of the μ-C_2 unit has important ramifications (vide infra).

Spectroscopic information about the bond order of the dicarbide unit was obtained via Raman spectra of **5** and $[(silox)_3Ta]_2(\mu\text{-}^{13}C_2)$ (**5**-$^{13}C_2$). A strong absorption at 1617 cm^{-1} was assigned to the symmetric C–C stretch of **5**, and a corresponding band at 1549 cm^{-1} (calcd, 1553 cm^{-1}) appeared in the spectrum of **5**-$^{13}C_2$. This absorption falls near the range of typical C=C bond stretches (1620–1680 cm^{-1}), thus corroborating the 1.37 (4) Å bond distance observed in the X-ray structural study.

Since the carbons of the μ-$^{13}C_2$ bridge of **5**-$^{13}C_2$ escaped detection via ^{13}C NMR and the remaining shifts hinted at paramagnetic character, a greater understanding of the electronic structure of the dicarbide was deemed necessary. Figure 2 illustrates a truncated version of the molecular orbital diagram corresponding to $[(HO)_3Ta]_2(\mu\text{-}C_2)$ (**5′**), a hypothetical model of $[(silox)_3Ta]_2(\mu\text{-}C_2)$ (**5**), as determined by an extended Hückel calculation. For calculational ease, the molecule was treated in its highest possible symmetry, D_{3d}. The left-hand side of the diagram shows the critical fragment MOs pertaining to the Ta···Ta (5.27 Å) interaction of an elongated $(HO)_3Ta\cdots Ta(OH)_3$ dimer; on the right are displayed the important orbitals of a slightly elongated (1.37 Å) dicarbon molecule. The molecular orbital

(45) (a) Schrock, R. R. *Acc. Chem. Res.* **1979**, *12*, 98–104. (b) Schultz, A. J.; Brown, R. K.; Williams, J. M.; Schrock, R. R. *J. Am. Chem. Soc.* **1981**, *103*, 169–176. (c) Chamberlain, L.; Rothwell, I. P.; Huffman, J. C. *Ibid.* **1982**, *104*, 7338–7340.

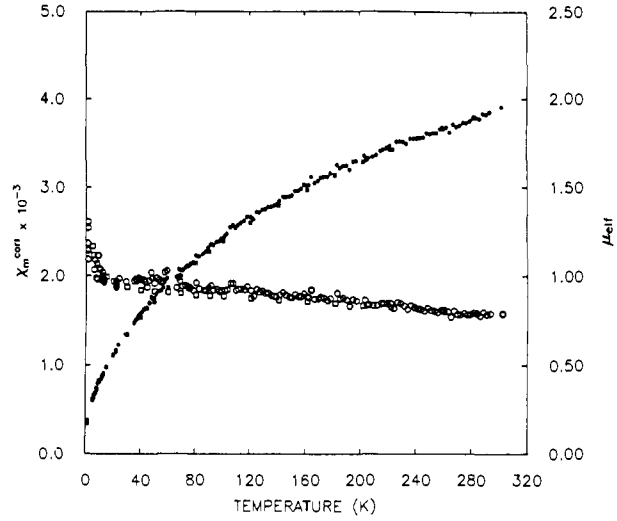

Figure 3. Corrected magnetic susceptibility (χ_m^{corr}; ○, □) and corresponding μ_{eff} (Bohr magnetons; ■, ●) vs T for $[(silox)_3Ta]_2(\mu\text{-}C_2)$ (**5**). The data were compiled from four independent experiments.

scheme of **5′** illustrates the frontier orbitals pertinent to the bonding of the dicarbide bridge. At the bottom is shown the uppermost σ^b ($1a_{1g}$) MO derived from the symmetric combination of two Ta d_{z^2} orbitals and the appropriate p_z-based dicarbon fragment; the remaining two σ-bonding MOs pertaining to the TaCCTa unit are much lower in energy and are not depicted. Since each $(silox)_3Ta$ moiety contains two d electrons, a total of 12 electrons occupy orbitals critical to the dicarbide bridge. Six of these are in σ orbitals, hence six are left for π bonding. In valence bond terms, the C–C and both Ta–C single bonds are accounted for. The next orbitals shown, the degenerate, π-bonding $1e_u$ set, result from combining the pair of symmetric Ta···Ta dπ orbitals with their $(p_x + p_x)$ and $(p_y + p_y)$ counterparts on dicarbon. The energy of the fully occupied $(1e_u)^4$ orbitals relative to the dicarbon π set reveals that it is mostly carbon in character (~80% C, 20% Ta), thus the electron density resides primarily amid the carbons. The $(e_g)^2$ orbitals, representing the HOMOs of the diagram, are another degenerate pair derived from the antisymmetric Ta···Ta dπ orbitals in combination with the $(p_x - p_x)$ and $(p_y - p_y)$ antibonding orbitals of C_2. Here the situation is reversed from the previous one; the MOs are distinctly tantalum in character (~80% Ta, ~20% C) and the probability of locating an electron is highest near the tantalums. Since only two electrons remain, the set is half-filled, resulting in three states: $^1A_{1g}$, ^1E_g, and $^3A_{2g}$. The paramagnetism of **5** can now be rationalized,[46] although its nature and the choice of the appropriate ground state are complicated.

A comparison of the molecular orbital description above with the valence bond interpretation of **5** as $(silox)_3Ta{=}C{=}C{=}Ta(silox)_3$ is interesting. Molecular orbital theory shows that the electronic situation is similar to $[RCCR]^{2+}$, because of the cylindrical symmetry of the D_{3d} complex, and offers a possible explanation for the paramagnetic nature of **5**. However, the IR and Raman stretching frequencies of the bridge components suggest that Ta=C (709 cm^{-1}) and C=C (1617 cm^{-1}) descriptions of the bonding are relevant. The MO diagram actually indicates a somewhat higher C–C bond order, but this prediction is strongly dependent on the choice of bond distances and the relative energies

(46) Upon extrapolation from the molecular orbital diagram of $[(HO)_3Ta]_2(\mu\text{-}C_2)$ (**5′**), the occupancy of the HOMO (half, $S = 1$; full, $S = 0$) for any cylindrically symmetric, linear carbide, $L_xMC_mML_x$, may be predicted for $L_xM = d^n$: (1) n is odd, m is odd, $S = 1$; m is even, $S = 0$; (2) n is even, m is odd, $S = 0$; m is even, $S = 1$; (3) for $n = 4$, m is even and $n \geq 5$, π^* orbitals are being populated. These rules assume that the general energetics of the bridge orbitals are as follows: σ^b ($n + 1$ single bonds, hence $2(n + 1)$ electrons) $< \pi^b < \pi^* < \sigma^*$. Note that this portrayal is predicated on a $1e^-$-type picture such as those generated in extended Hückel calculations. As is seen for **5**, the predicted spin values may not accurately describe the true ground state of the complex since electron–electron correlations are not included.

of the $(HO)_3Ta\cdots Ta(OH)_3$ and C_2 fragments that are employed. Problems such as these are common to the extended Hückel method and could possibly be minimized if more accurate parameters (e.g., orbital basis sets, bond distances, etc.) were utilized. Since an MO representation of **5** is more difficult to illustrate and the valence bond interpretation has merit, the latter depiction of the dicarbide will be used throughout the schemes in the text.

The ambiguity pertaining to the choice of ground states that can be assigned to the $(e_g)^2$ configuration (^1E_g, $^1A_{1g}$ or $^3A_{2g}$) in Figure 2 was partially alleviated by magnetic measurements. In the preliminary report,[28] a 25 °C measurement by the Faraday method indicated that $\mu_{eff} = 3.0\ \mu_B$, interpreted as an indication of a triplet ground state. Subsequent investigations from 2 to 300 K and 25 °C variable-field studies revealed that the magnetism of **5** is more complex. Figure 3 illustrates the temperature vs corrected magnetic susceptibility, χ_m^{corr}, which includes subtractions of contributions from diamagnetism and an unexpected field dependence. The latter, presumably due to ferromagnetic impurities, was corrected for by the Honda–Owens method.[47] The figure also manifests the dependence of μ_{eff} on temperature. This curve establishes the ground state of the dicarbide (**5**) as a singlet, either ^1E_g or $^1A_{1g}$, since μ_{eff} approaches zero at 0 K. The slight discrepancy from zero is likely due to the presence of a small paramagnetic impurity, also observed as an obvious low-temperature (2–20 K) Curie–Weiss tail superimposed on a strikingly temperature-independent susceptibility (χ_m^{corr}). Accordingly, this temperature-independent paramagnetism (TIP) is also evidenced via the correlation of μ_{eff} with $T^{1/2}$.[48,49]

The observation of a magnetic susceptibility occurs when a system undergoes a change in energy upon placement in a magnetic field. For the observation of *only* a large TIP, the applied field must induce extensive orbital mixing between ground-state singlet and paramagnetic excited states.[49] The mixing occurs via the second-order Zeeman terms in the expression for the energy of an electronic level in a magnetic field. The lack of T dependence on χ_m^{corr} indicates that these states must be energetically far enough apart to obviate thermal population ($\Delta E = E_{GS} - E_{ES} \gg kT$; $\Delta E \sim 1000\ cm^{-1}$).[50] Since the states involved are derived from the same e_g^2 configuration, their orbital components must be comprised of the same basis functions, the Ta d_{xz}, d_{yz} and carbon p_x, p_y atomic orbitals (Figure 2). It is therefore not surprising that **5** exhibits such a large TIP; similar factors result in large TIP values for other third row (e.g., $K_2[OsCl_6]$) and lanthanide complexes.[49] Attempts to examine $[(silox)_3Ta]_2(\mu\text{-}C_2)$ (**5**) by EPR spectroscopy have been clouded by the ferromagnetic impurities. Nonetheless, no resonances that could be attributed to **5** have been observed, consistent with the above. The UV–vis spectrum of **5** is equally uninformative, manifesting a broad manifold of absorptions in the 350–600-nm (ϵ = 3000–6000 cm^{-1} M^{-1}) region, typical IL and LMCT bands (214 nm (~15 000), 256 (9000), 280 (11 000), 310 (52 000)).[51]

Perhaps the answer to why dicarbide **5** possesses a singlet ground state rather than the triplet is indicated by the apparent distortion of the TaCCTa bridge ($\angle$TaCC = 173 (3)°). Whereas the $^1A_{1g}$ state is orbitally symmetric, the ^1E_g state is subject to a first-order Jahn–Teller effect,[52] relieving the degeneracy. Although a truly linear μ-C_2 bridge is still within 3σ of the stated value, the crystallographic point group symmetry of **5** is clearly $\bar{1}$, a necessary consequence of such a distortion, but insufficient proof of its existence.[53] The X-ray structural depiction reveals an overal symmetry of C_i and a local symmetry of C_{2h}, inducing a splitting of the orbitally degenerate ^1E_g state to two ^1A_g levels in the former and a ^1A_g and ^1B_g in the latter. In C_i, the $^1A_{1g}$ and $^3A_{2g}$ states become ^1A_g and ^3A_g, and in C_{2h}, these levels are ^1A_g and ^3B_g. In either instance, it is clear that configuration interactions, expected to be strong, could mitigate any thermal population of paramagnetic excited states (i.e., antiferromagnetism) in accord with the observed T independence.[50]

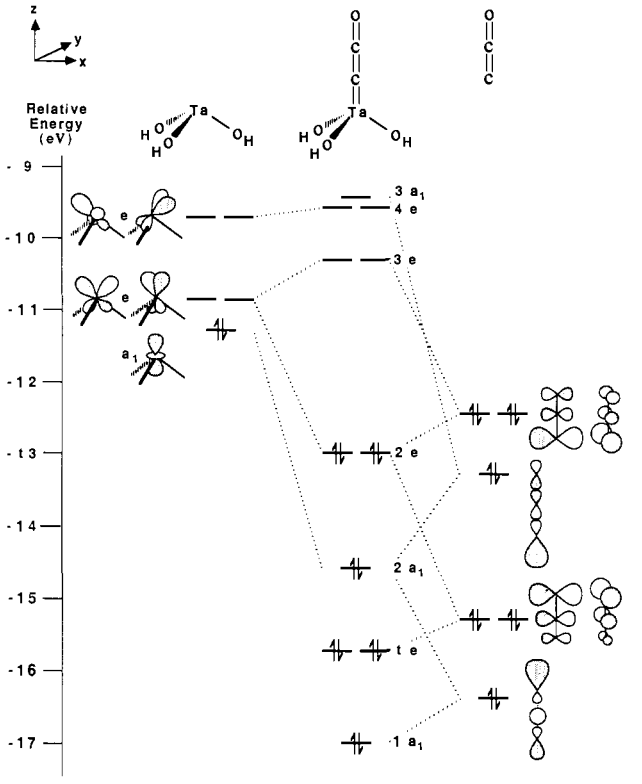

Figure 4. Truncated molecular orbital diagram of $(HO)_3Ta{=}C{=}C{=}O$ (**6′**), a model of $(silox)_3Ta{=}C{=}C{=}O$ (**6**).

(silox)$_3$Ta=C=C=O (6). The presence of impurity oxo (**3**) prevented characterization of $(silox)_3Ta{=}C{=}C{=}O$ (**6**) by X-ray diffraction methods; thus, the aforementioned spectroscopic data served as proof of its structure. Extended Hückel calculations were carried out to ascertain the nature of the CCO ligation.[40,41,54] As Figure 4 illustrates, the $(silox)_3Ta$ portion of the molecule was modeled by $(HO)_3Ta$, which was pyramidalized according to the structural parameters of the dicarbide (**5**). Reasonable bond distances for the CCO (d(C=C) = 1.32 Å, d(C=O) = 1.16 Å) and Ta=C (1.97 Å) units were employed. The truncated molecular orbital diagram of $(HO)_3Ta{=}C{=}C{=}O$ (**6′**) is very similar to that of dicarbide **5**, but with four additional electrons, since the d^2 $(HO)_3Ta$ center of **5** is "replaced" by an oxygen atom (six electrons). Two of the e$^-$'s occupy the $1a_1$ orbital, essentially an oxygen "lone pair", that has no counterpart in **5**. The HOMOs of **6** constitute a degenerate set of π^b-type orbitals (2e) that are mostly C_α localized, while the LUMOs (3e) are metal localized and similar to the $2e_u$ LUMOs of **5**. Although the 3e MOs of **6** are distinctly Ta centered, appreciable C_β character is also evident due to some mixing with the highest π^* orbital of CCO (not depicted). The α-carbon-centered 2e set, which contrasts with the metal-localized e_g of **5**, is derived from a relatively nonbonding CCO orbital that is energetically close. Recall that

(47) Bates, L. F. *Modern Magnetism*; 3rd ed.; Cambridge University Press: London, 1951.

(48) (a) Carlin, R. L. *Magnetochemistry*; Springer-Verlag: New York, 1977. (b) Carlin, R. L.; van Duyneveldt, A. J. *Magnetic Properties of Transition Metal Compounds*; Springer: New York, 1977. (c) Drago, R. S. *Physical Methods in Chemistry*; Saunders: Philadelphia, PA, 1977.

(49) Figgis, B. N. *Introduction to Ligand Fields*; John Wiley & Sons: New York, 1966; pp 248–292.

(50) It is possible that a small contribution from thermally accessible excited states is present. The values of χ_m^{corr} are not rigorously T independent; the slope of χ_m^{corr} vs T is small ($\sim -1 \times 10^{-6}$/K) yet noticeable.

(51) The assignments of the LMCT and IL absorptions are based on the observation of similar bands in **4**, related monomeric d^0 species (see ref 16), and a 213-nm absorption in Na(silox) that can be attributed to an O($p\pi$) → Si(d^*) transition.

(52) (a) Jahn, H. A.; Teller, E. *Proc. R. Soc. London, A* **1937**, *161*, 220–235. (b) Jahn, H. A. *Ibid.* **1938**, *164*, 117–131.

(53) For example, the bridge could be truly linear and the critical orbitals degenerate, yet the periphery could dictate the lower symmetry C_i.

(54) D'Agostino, M. F.; Mlekuz, M.; Kolis, J. W.; Sayer, B. G.; Rodger, C. A.; Halet, J.-F.; Saillard, J.-Y.; McGlinchey, M. J. *Organometallics* **1986**, *5*, 2345–2350.

the HOMO of **5** originates from the C–C π^* orbital of dicarbon.

As a consequence of its C_α-localized HOMO and cumulene-like nature, **6** may not be structurally analogous to organic ketenes. A bending of the Ta–C_α–C_β angle would disrupt the degeneracy of the 2e set and allow mixing with the a_1 MOs. Cluster M_3-(μ_3-CCO) moieties display linear CCO units that are tilted with respect to the M_3 plane,[40,41,54] and nonlinear binding by the CCX groups of phosphacumulene ylides contributes to their stability. The degree to which these fragments are bent ($Ph_3P{=}C{=}C{=}X$, X = S, O, NR, $(OEt)_2$: ∠PCC = 168–126°), and the different reactivity patterns observed, depend on the π-accepting/π-donating properties of the X group.[55] In a series of calculations, the CCO group of **6** was allowed to bend from 0° (linear) to a Ta–C_α–C_β angle of 30°. Although the linear form was of lowest energy, deviations from 0° are not energetically costly; at 30°, the bent structures, either toward or away from a TaOH linkage, were only 4 kcal/mol higher, suggesting that the C_α could act in a nucleophilic manner. In contrast, if the TaCCO unit was kept linear and bent toward or away from a TaOH group, the potential energy surface was substantially steeper. Destabilization due to loss of π bonding results in a 4 kcal/mol increase in energy after deviations of only 15°; at this point the slopes of the potential energy curves rapidly increased and further canting of the TaCCO unit was deemed unlikely.

In summary, although deviations from $TaC_\alpha C_\beta O$ linearity are plausible, the ketenylidene ligand should react similarly to an organic ketene. The β-carbon possesses electrophilic and the α-carbon nucleophilic character, as observed for their organic counterparts.[56] However, the effect of the steric congestion about the ligand undoubtedly plays the major role in the chemistry of **6**. For example, dimerization of $(silox)_3Ta{=}C{=}C{=}O$ (**6**), which would be expected on the basis of the organic analogy, does not occur.

Mechanistic Investigations

Carbonyl Complexes. Even under optimum conditions for $[(silox)_3Ta]_2(\mu\text{-}C_2)$ (**5**) formation (eq 5), trace amounts of $(silox)_3TaCCO$ (**6**) were detected by infrared spectroscopy. Coupled with the appearance of trace amounts of **5** during procedures maximizing ketenylidene **6** (eq 8), these observations implicate the latter as an intermediate on the path to dicarbide. Based on this assumption, an investigation into the formation of **6** was conducted. Logically, an initial step of the process would involve a carbonyl adduct of $(silox)_3Ta$ (**2**). In nondonor solvents such as toluene, benzene, hexane, and Et_2O, $(silox)_3TaCO$ (**2**-CO) was not observed spectroscopically or visually at −78 °C. Instead, a red precipitate, shown *not* to be dicarbide **5**,[57] was generated within 30 min;[58] upon warming, this species produced **6** and $(silox)_3Ta{=}O$ (**3**).

Fortunately, carbonylation of $(silox)_3Ta$ (**2**) in certain donor solvents (e.g., THF, DME, 2-Me-THF) led to thermally unstable, solvated CO adducts. For example, an uptake of 0.97 equiv of CO was observed when **2** was carbonylated (1 atm, 15 min) in THF at −78 °C, resulting in a yellow solution containing $(silox)_3(THF)TaCO$ (THF-**2**-CO) (eq 9). At −110 °C, the ^1H

$$\underset{\mathbf{2}}{(silox)_3Ta} + CO \xrightarrow[-78\ ^\circ C]{THF} \underset{\text{THF-}\mathbf{2}\text{-CO}}{(silox)_3(THF)TaCO} \qquad (9)$$

NMR spectrum of THF($-d_8$)-**2**-CO consists of two broad silox resonances at δ 12.4 ($\nu_{1/2}$ = 200 Hz) and 7.7 ($\nu_{1/2}$ = 90 Hz) that appear in a 2:1 ratio in THF-d_8. Upon warming, the two resonances shift upfield, as expected for a simple paramagnetic species,[59] and coalesce at −80 °C ($k_c \sim 1.4\ (2) \times 10^3\ s^{-1}$, $\Delta G^\ddagger$ = 8.4 (1) kcal/mol, 400 MHz). Although several square-pyramidal structures could account for the inequivalence of the silox groups, molecular models clearly indicate that every SiO–Ta–OSi angle must approach 120°, leading to a trigonal-bipyramidal (TBP) arrangement. The different silox resonances could arise from a configurationally locked THF ligand. Substantial π donation by the THF would render the Ta–THF plane relatively flat, as observed in other early metal THF complexes.[60] From inspection of molecular models, it is likely that the hydrocarbon backbone of THF may slide between two silox ligands while abutting the third (I), or align in separating two of the silox groups from the other (II), as Figure 5 illustrates. Slight deviations from TBP geometry would not be expected to split the half-occupied d_{xz} and d_{yz} orbitals enough to cause spin-pairing, consistent with the paramagnetism observed. A trans-axial disposition of the π-donating THF and π-accepting CO ligands is supported by a low CO stretch at 1840 cm^{-1} ($\nu(^{13}CO)$ = 1796; calcd, 1799 cm^{-1}) in the −77 °C infrared spectrum of THF-**2**-CO. The dynamic equilibration of the silox units probably arises from a geared rotation of the THF ligand, not through a dissociative exchange with free solvent (vide infra). The coalescence rate is not THF-dependent, as judged from measurements conducted in varying concentrations of THF-d_8/methylcyclohexane-d_{14},[61] and thus an associative THF exchange is considered unlikely.

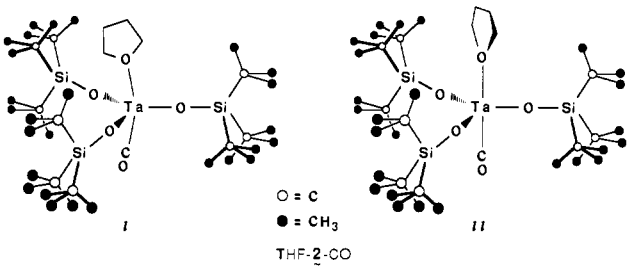

Figure 5. Possible THF orientations in $(silox)_3(THF)TaCO$ (THF-**2**-CO).

The arguments above presuppose that THF is actually binding to the tantalum center. Aggregates of $(silox)_3TaCO$ (**2**-CO) or a slowly equilibrating mixture of carbonylates could also lead to inequivalent silox groups. Several factors conflict with these hypotheses: (1) neither the position nor rate of coalescence seems to depend on initial $(silox)_3Ta$ (**2**) concentration, although the experimental conditions could not be widely varied; (2) the complex exhibits only one carbonyl band (1840 cm^{-1}) in the −70 °C IR spectrum; (3) exposure of **2** to CO in 2,5-dimethyl-THF, a poor donor, resulted in the red precipitate without any indication of an intermediate carbonyl species. Since the dielectric constants of THF and 2,5-dimethyl-THF are nearly equal,[62] the observations above *cannot* simply be due to a medium effect.

In accord with the depiction in Figure 5, molecular models support a monomeric structure for $(silox)_3(THF)TaCO$ (THF-**2**-CO). Labeling experiments, while not definitive, also lend credence to this formulation. Solutions of THF-**2**-CO and THF-**2**-^{13}CO, independently generated and pumped free of residual carbon monoxide, were combined at −78 °C and allowed to warm. This crossover experiment produced a statistical mixture of **6**, (**6**-^{13}CC), (**6**-$C^{13}C$), and **6**-$^{13}C_2$ along with the corresponding

(55) Albright, T. A.; Hofmann, P.; Rossi, A. R. *Z. Naturforsch.* **1980**, *35B*, 343–351, and references therein.

(56) Patai, S., Ed. *The Chemistry of Ketenes, Allenes and Related Compounds*; Wiley: New York, 1980.

(57) $[(silox)_3Ta]_2(\mu\text{-}C_2)$ (**5**) does *not* react with CO at −78 °C or higher to give the red precipitate or ketenylidene **6**.

(58) Some red precipitate is observed immediately upon carbonylation of $(silox)_3Ta$ (**2**) in hexane solution at −78 °C, but complete formation of this intermediate requires an additional 30 min. Either CO dissolution in hexane is slow at −78 °C or a slight barrier to the formation of the CO adduct exists.

(59) A plot of $1/T$ (163–233 K) vs chemical shift for the ^{t}Bu resonance(s) attributable to $(silox)_3(THF)TaCO$ (THF-**2**-CO) was linear, thus corroborating the contention that THF-**2**-CO is a simple paramagnetic complex. See: LaMar, G. N.; Horrocks, W. D. W., Jr.; Holm, R. H. *NMR of Paramagnetic Molecules: Principles and Applications*; Academic Press: New York, 1973; p 11.

(60) (a) Jordan, R. F.; Bajgur, C. S.; Willett, R.; Scott, B. *J. Am. Chem. Soc.* **1986**, *108*, 7410–7411. (b) Walsh, P. J.; Hollander, F. J.; Bergman, R. G. *Ibid.* **1988**, *110*, 8729–8731. (c) Cummins, C. C.; Van Duyne, G. D.; Wolczanski, P. T., unpublished results.

(61) The use of methylcyclohexane-d_{14} was prompted by problems concerning overlapping resonances of C_7D_8 and the high freezing points of other typical deuterated hydrocarbons.

(62) Wax, M. J.; Bergman, R. G. *J. Am. Chem. Soc.* **1981**, *103*, 7028–7030.

Scheme I

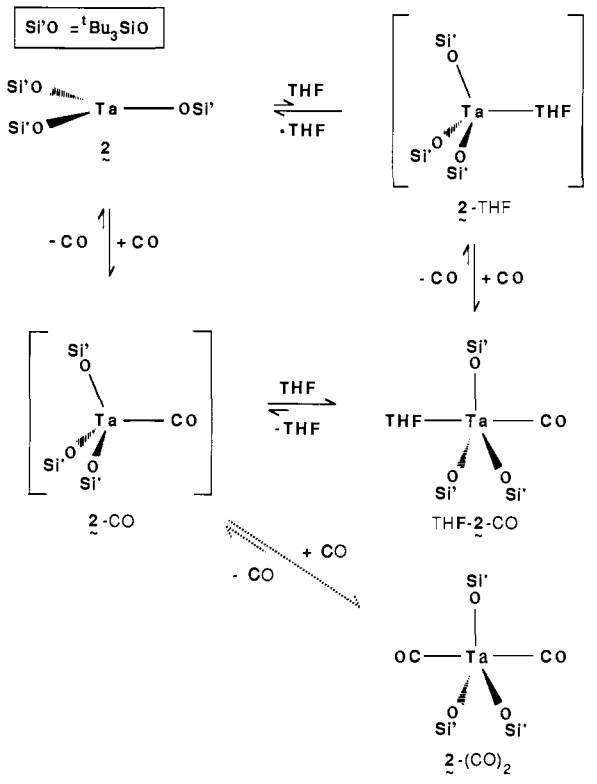

oxo **3**. Reactivity of this type would be expected for a *monomeric* monocarbonyl that aggregates to form the red precipitate, which subsequently breaks up to give **6** and **3**. In separate experiments, CO (450 Torr) was shown to only partially exchange with the labeled carbonyl of (silox)$_3$(THF)Ta^{13}CO (THF-**2**-^{13}CO) on the same time scale (~10 min) as the crossover, thus the previous results cannot be solely attributed to rapid dissociative CO exchange among carbonylates.

When a dilute solution of (silox)$_3$(THF)TaCO (THF-**2**-CO) was held at −78 °C for 1 h with excess CO (1 atm), its IR absorption decayed in a first-order process (−63 °C, k = 8.2 (5) × 10^{-4} s^{-1}) as another at 1870 cm^{-1} ($\nu(^{13}CO)$ = 1832; calcd, 1828 cm^{-1}), assigned to (silox)$_3$Ta(CO)$_2$ (**2**-(CO)$_2$), grew in (k = 8.5 (8) × 10^{-4} s^{-1}, eq 10). The yellow solution appeared to darken

$$\underset{\text{THF-2-CO}}{(\text{silox})_3(\text{THF})\text{TaCO}} + \text{CO} \xrightarrow[-78\ ^\circ\text{C}]{\text{THF}} \underset{\text{2-(CO)}_2}{(\text{silox})_3\text{Ta(CO)}_2} \qquad (10)$$

as THF-**2**-CO was converted to **2**-(CO)$_2$. A trigonal-bipyramidal structure for **2**-(CO)$_2$ is consistent with one CO band, and the increase in its stretching frequency relative to THF-**2**-CO reflects the presence of trans-axial carbonyls. No corroborating NMR evidence for this presumably paramagnetic dicarbonyl (**2**-(CO)$_2$) was obtained.[63] Because the rates of disappearance of THF-**2**-CO and appearance of **2**-(CO)$_2$ are first-order in [Ta] and appear independent of [CO], it is likely that THF loss from THF-**2**-CO governs the conversion. Assuming this mechanism and crudely extrapolating to −80 °C, the rate of THF loss from THF-**2**-CO is estimated to be 3 × 10^{-4} s^{-1},[64] a factor of ~10^6 slower than the silox equilibration rate obtained via the coalescence experiments. Recall that the latter are believed to reveal a THF rotation process.

Scheme I summarizes the nondonor and THF pathways leading to (silox)$_3$TaCO (**2**-CO), one probable precursor to the red precipitate, as exemplified by the sterically most probable TBP solvate. The data support the existence of (silox)$_3$(THF)TaCO (THF-**2**-CO), formed via either of two pathways: (1) a THF solvate, (silox)$_3$Ta(THF) (**2**-THF), could be trapped by CO, and (2) an initial CO adduct, (silox)$_3$TaCO (**2**-CO), could be trapped by THF. Recall that (silox)$_3$Ta (**2**) possesses a diamagnetic ground state in accord with a filled d_{z^2} orbital. As has been noted previously,[65,66] electron–electron repulsions resulting from interactions of Ta orbitals possessing d_{z^2} character and a σ orbital of a weak donor ligand (i.e., THF) discourage binding via the latter. In support, UV–vis spectra of **2** in CyH and THF are virtually identical, and thus no spectroscopic evidence for **2**-THF has been noted. Furthermore, pathway 2 is favored because the 4e$^-$ repulsion problems may be overcome if a strong π-acceptor (i.e., CO) substantially aids in lowering the energy of the d_{xz}, d_{yz} orbitals, which are the HOMOs of the initial C_{3v} adduct. Sizable back-bonding to the carbonyl in THF-**2**-CO, as indicated by its 1840-cm^{-1} CO stretch, suggests that a similar strong interaction would be present in **2**-CO. Since the LUMO of **2**-CO is predominantly d_{z^2} in character, CO binding may actually activate the tantalum center toward acceptance of a σ-donor (i.e., THF). Finally, these arguments are also consistent with the ultimate formation of (silox)$_3$Ta(CO)$_2$ (**2**-(CO)$_2$) with excess carbon monoxide, because CO is strong π-acceptor and a weaker σ-donor than THF.

Scheme II

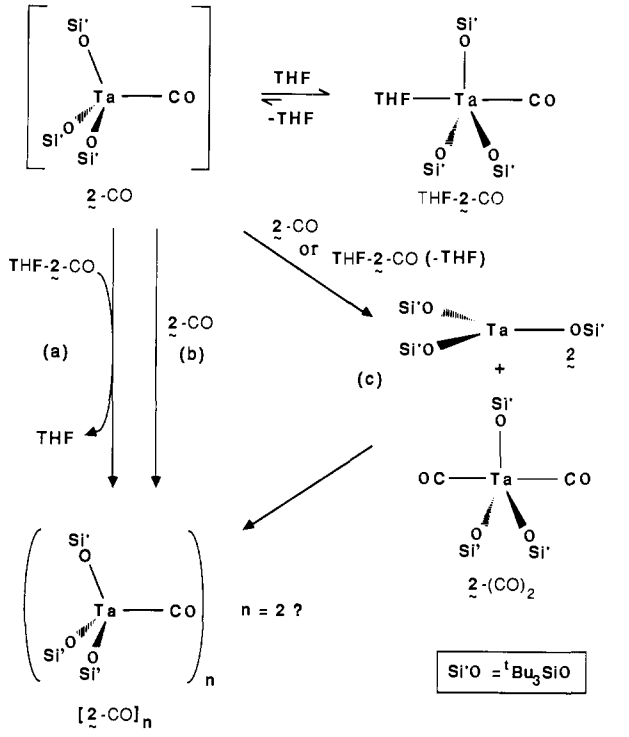

Ketenylidene (6) Formation. Direct characterization of the intermediate red precipitate has been difficult to obtain, since its decomposition to ketenylidene **6** and oxo **3** occurs even in the solid state if the complex is not kept cold (−78 °C). The structure of (silox)$_3$Ta=C=C=O (**6**) suggests that its precursor contains at least two (silox)$_3$TaCO units and no observation of solvent binding to this precipitate has been made. Logically, dimerization of (silox)$_3$(THF)TaCO (THF-**2**-CO) could occur via initial loss of

(63) Relatively high concentrations (e.g., 0.02 M) are needed to be confident of observing paramagnetic species such as THF-**2**-CO and **2**-(CO)$_2$. At these concentrations, the reaction of THF-**2**-CO to form the red precipitate, [(silox)$_3$TaCO]$_n$ ([**2**-CO]$_n$), competes effectively with further carbonylation to give **2**-(CO)$_2$.

(64) These arguments are based on the adage that the rate of a typical first-order process will double every 10 °C.

(65) Neithamer, D. R.; Párkányi, L.; Mitchell, J. F.; Wolczanski, P. T. *J. Am. Chem. Soc.* **1988**, *110*, 4421–4423.

(66) Calculations have shown that a severe four-electron, two-orbital destabilization of a σ-donor orbital occurs because of a strong interaction with a low-lying, symmetric σ combination localized on the three oxygens of the silox groups. This destabilizing interaction is primarily responsible for the η^2 rather than η^1 binding of pyridine to (silox)$_3$Ta (**2**; see ref 65). (a) Neithamer, D. R.; Zonnevylle, M. C.; Párkányi, L.; Wolczanski, P. T., manuscript in preparation. (b) Zonnevylle, M. C. Ph.D. Thesis, Cornell University, Ithaca, NY, 1989.

Scheme III

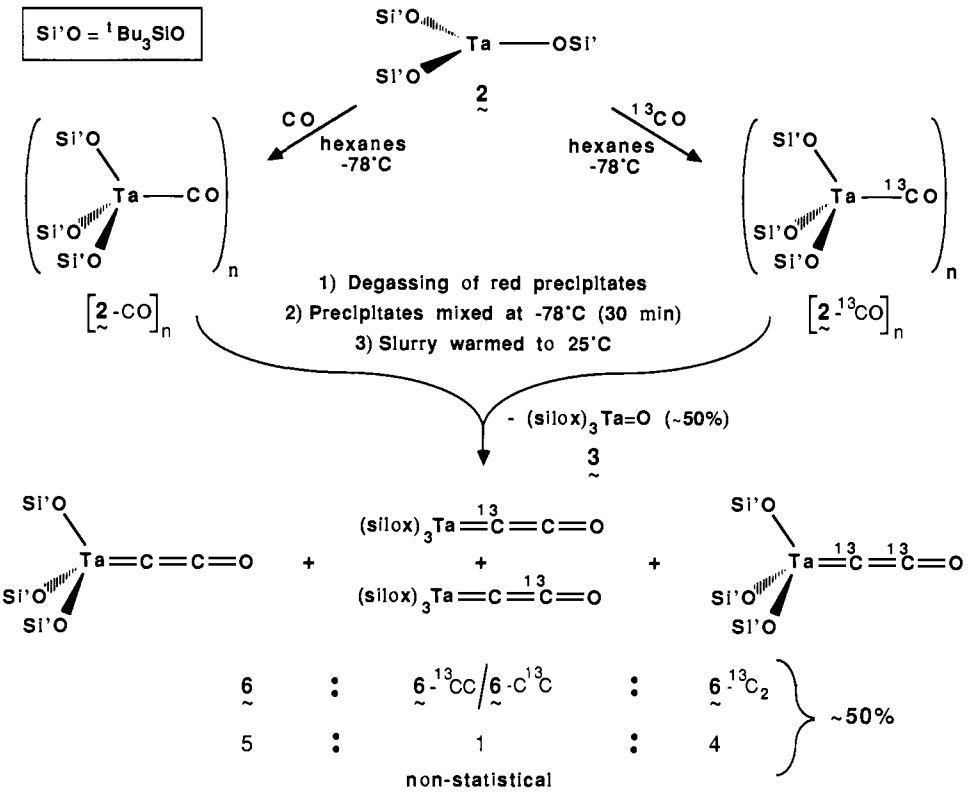

THF, followed by capture of $(silox)_3TaCO$ (**2**-CO) by THF-**2**-CO (Scheme II, path a) or another **2**-CO (path b) to form the ketenylidene precursor, tentatively formulated as $[(silox)_3TaCO]_n$ ($[\mathbf{2}\text{-CO}]_n$). Another plausible mechanism involves the disproportionation of **2**-CO (or **2**-CO and THF-**2**-CO) to give $(silox)_3Ta$ (**2**) and $(silox)_3Ta(CO)_2$ (path c), which then quickly recombine, producing $[\mathbf{2}\text{-CO}]_n$. Provided the loss of THF from THF-**2**-CO is fast and reversible, the disappearance of THF-**2**-CO in each case is predicted to be second order. Corroboration was obtained through monitoring the decline of [THF-**2**-CO] in the ^1H NMR at −63 °C ($k \geq 0.5$ (1) M^{-1} s^{-1}) and −71 °C ($k \geq 0.2$ (1) M^{-1} s^{-1}).[67] Unfortunately, significant variation in the concentration of THF-**2**-CO could not be accomplished due to the rapidity of $[\mathbf{2}\text{-CO}]_n$ formation at high concentrations and integration difficulties at low concentrations. Note that path b requires loss of THF from two THF-**2**-CO species prior to the second-order step while path a requires only one, suggesting a differentiation based on either first- (a) or second- (b) order[68] inhibition by THF. Kinetics experiments using THF-d_8/methylcyclohexane-d_{14}[61] solvent mixtures were attempted and an obvious acceleration in rate was observed; however, quantitative data could not be obtained due to this rapid increase. In order to ascertain that the species monitored by ^1H NMR (presumably $(silox)_3(THF)TaCO$ (THF-**2**-CO)) was the same as that possessing the aforementioned 1840-cm^{-1} IR band, the disappearance of the latter absorbance was followed. At −72 °C, the CO stretch diminished at a rate of ≥0.4 (1) M^{-1} s^{-1}, although the differences in the first- and second-order fits were somewhat ambiguous. Nonetheless, the quantitative comparison with the NMR kinetics corroborates the implication of THF-**2**-CO as the precursor to the red precipitate. An attempt to differentiate path c from paths a/b by allowing THF-**2**-^{13}CO to warm in the presence of independently generated **2**-$(CO)_2$ failed due to scrambling processes. While not entirely definitive, in total these studies support the contention that THF loss occurs prior to or during the second-order and probably rate-determining step.

The possibility that $(silox)_3Ta(CO)_2$ (**2**-$(CO)_2$) is directly involved (path c) in the formation of $[(silox)_3TaCO]_n$ ($[\mathbf{2}\text{-CO}]_n$) could not be experimentally ruled out, but its stability suggests that it is a byproduct that can serve as a source of **2**-CO. During IR experiments monitoring the rate of disappearance of THF-**2**-CO, dicarbonyl **2**-$(CO)_2$ was present in different concentrations that remained invariant over the course of each run; the observed rates were unaffected. Furthermore, **2**-$(CO)_2$ is stable at −25 °C for several hours, whereas THF-**2**-CO decays rapidly to $[\mathbf{2}\text{-CO}]_n$ at −72 °C. Thus, excess CO inhibits the formation of $[\mathbf{2}\text{-CO}]_n$ by diverting the course of reaction to dicarbonyl, **2**-$(CO)_2$. Presumably, after THF-**2**-CO loses solvent, CO scavenges the empty site faster than second-order processes occur to give $[\mathbf{2}\text{-CO}]_n$. Although THF-**2**-CO effectively captures solvated free CO, Toepler pump experiments showed that **2**-$(CO)_2$ lost CO under vacuum. Interestingly, dicarbonyl **2**-$(CO)_2$ may play a more important role in hydrocarbon or noncoordinating solvents. Recall that **2**-CO is predicted to be activated for attack by another donor (vide supra). It is therefore conceivable that CO preferentially binds to transient **2**-CO rather than $(silox)_3Ta$ (**2**) in noncoordinating media, and that coupling of the CO ligands on **2**-$(CO)_2$ upon attack by **2**[30-32] leads to $[\mathbf{2}\text{-CO}]_n$.

The preceding studies set the stage for investigation of the decomposition of $[(silox)_3TaCO]_n$ ($[\mathbf{2}\text{-CO}]_n$), the red precipitate. Scheme III illustrates the first of two critical labeling experiments which strongly suggest that the CC bond has already been formed in $[\mathbf{2}\text{-CO}]_n$, and that n is likely to be 2. In separate flasks, $[\mathbf{2}\text{-CO}]_n$ and $[\mathbf{2}\text{-}^{13}CO]_n$ were generated in hexanes at −78 °C and then intimately mixed for 30 min at that temperature. The slurry was permitted to warm to 25 °C and the product ketenylidenes were shown to be a *nonstatistical* 5:1:4 mixture of **6**:(**6**-^{13}CC)/(**6**-C^{13}C):**6**-$^{13}C_2$, indicative of ≤5% crossover after correction for the use of 90% labeled ^{13}CO. In Scheme IV, free CO was shown not to incorporate into the framework of ketenylidene generated from $[\mathbf{2}\text{-}^{13}CO]_n$ since greater than 95% $(silox)_3Ta{=}^{13}C{=}^{13}C{=}O$ (**6**-

(67) Attempts to plot the data in accord with a first-order disappearance of [THF-**2**-CO] revealed significant deviations from linearity (see supplementary material). However, the second-order rates obtained in these experiments must be considered lower limits. Some of the red precipitate, $[(silox)_3TaCO]_n$ ($[\mathbf{2}\text{-CO}]_n$), was observed to be present in the NMR tubes prior to the start of each kinetics run; thus, the $t = 0$ s concentrations of THF-**2**-CO were somewhat less than that measured prior to ^1H NMR monitoring.

(68) Only in the case of rapid, reversible THF loss from THF-**2**-CO must path b be rigorously inverse second order in THF.

Scheme IV

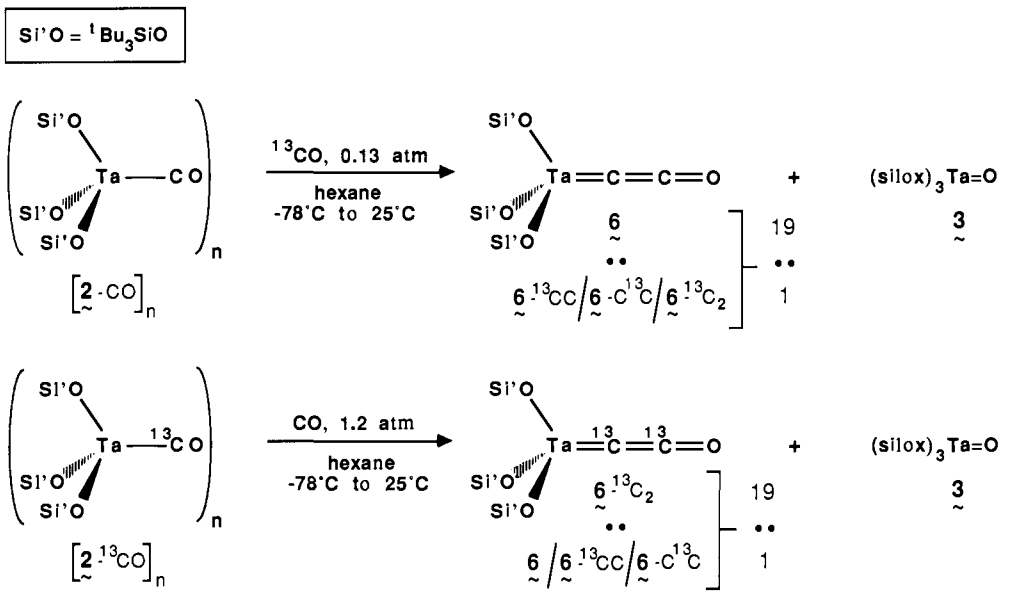

$^{13}C_2$) was observed. In the complementary labeling assay, ≥95% **6** formed when [**2**-CO]$_n$ was warmed under an atmosphere of ^{13}CO. Again, these percentages contain corrections for 90% labeled ^{13}CO use. Furthermore, when [**2**-CO]$_n$ was extensively washed with hexanes at −78 °C, the filtrates contained no (silox)$_3$Ta=O (**3**). Since **3** is soluble in hexane, even at −78 °C, formation of [**2**-CO]$_n$ has occurred without deoxygenation of CO.

In total, these experiments show that the ketenylidene (**6**) and oxo (**3**) are derived from the same aggregate, [**2**-CO]$_n$. Since the studies show that [**2**-CO]$_n$ does not dissociate CO or deaggregate to **2**-CO on the path to ketenylidene, they strongly imply that the carbon–carbon linkage has been established in a structure where both C–O bonds have not yet been completely severed. Furthermore, an assessment of steric complications provided by molecular models reveals a clear bias toward dimeric formulations, with the only possible exception being an unlikely linear arrangement of **2**-CO groups (Ta–CO···(Ta–CO···)$_{n-2}$···Ta–CO). Figure 6 exhibits possible structures for the red precipitate, [**2**-CO]$_n$, that are consistent with the discussion above where n = 2. One favored orientation is manifested in A, where a decomposition (dashed lines) reminiscent of those pertaining to metallacyclobutanes leads directly to ketenylidene (**6**) and oxo (**3**). This intermediate is most appealing because a simple, two-step process to **6** and **3** can be envisioned: a coupling of **2**-CO fragments to give A, followed by a breakup of the latter as indicated. Degradation of carboxylate-like B, a structure similar to Evan's ketenecarboxylate dimer,[27] would lead to the correct products, but in this case the critical C–O bond has already been broken at −78 °C. The slightly longer μ-O$_2$CC bridge of the latter presents a steric advantage over A. Deoxygenation of the symmetrically bridged, coupled-carbonyl[30–32] structure C would lead to a carbene fragment that would be subject to rearrangement (vide infra) to give **6**. This geometry is attractive since the (silox)$_3$Ta centers are about as far apart as in the dicarbide (**5**), whereas A forces the tantalums even closer. Although D violates the contentions regarding C–C bond formation, it nonetheless bears mentioning given the steric problems confronted in coupling two (silox)$_3$TaCO (**2**-CO) units.

Dicarbide (5) Formation. When (silox)$_3$Ta=C=C=O (**6**) was treated with 2.0 equiv of (silox)$_3$Ta (**2**), the dicarbide, [(silox)$_3$Ta]$_2$(μ-C$_2$) (**5**), and oxo, (silox)$_3$Ta=O (**3**), were formed according to eq 11. Scheme V indicates a plausible sequence

$$\underset{\mathbf{6}}{(\text{silox})_3\text{Ta}{=}\text{C}{=}\text{C}{=}\text{O}} + 2\underset{\mathbf{2}}{(\text{silox})_3\text{Ta}} \xrightarrow{25\ ^\circ\text{C}} \underset{\mathbf{5}}{[(\text{silox})_3\text{Ta}]_2(\mu\text{-C}_2)} + \underset{\mathbf{3}}{(\text{silox})_3\text{Ta}{=}\text{O}} \quad (11)$$

of reactions that delineate this transformation: (1) ketenylidene **6** forms an initial adduct with **2**, (silox)$_3$Ta=C=C(–O–Ta(silox)$_3$)=O (**6**·**2**); (2) deoxygenative degradation of the adduct yields oxo **3** and a transient vinylidene (silox)$_3$Ta=C=C: (**2**-C$_2$); (3) **2**-C$_2$ is then capped by a second (silox)$_3$Ta (**2**) to produce dicarbide **5**. As predicted in this depiction, the C=C bond of the ketenylidene (**6**) remains intact during the deoxygenation process, as shown via a crossover experiment. Treatment of a 1:1 mixture of **6** and (silox)$_3$Ta=^{13}C=^{13}C=O (**6**-^{13}C$_2$) with **2** generated only **5** and [(silox)$_3$Ta]$_2$(μ-^{13}C$_2$) (**5**-^{13}C$_2$) as shown in eq 12.

$$\underset{\mathbf{6}}{(\text{silox})_3\text{Ta}{=}\text{C}{=}\text{C}{=}\text{O}} + \underset{\mathbf{6}\text{-}^{13}\text{C}_2}{(\text{silox})_3\text{Ta}{=}{}^{13}\text{C}{=}{}^{13}\text{C}{=}\text{O}} \xrightarrow[-2(\text{silox})_3\text{Ta}{=}\text{O}\ (\mathbf{3})]{4(\text{silox})_3\text{Ta}\ (\mathbf{2})} \underset{\mathbf{5}}{[(\text{silox})_3\text{Ta}]_2(\mu\text{-C}_2)} + \underset{\mathbf{5}\text{-}^{13}\text{C}_2}{[(\text{silox})_3\text{Ta}]_2(\mu\text{-}^{13}\text{C}_2)} \quad (12)$$

Spectroscopic evidence for an adduct such as **6**·**2** has not been obtained, but an analogous diphenylketene complex,[69] (silox)$_3$Ta(–O–C=CPh$_2$) (**7**), was isolated as bright yellow microcrystals (40% yield) from addition of OCCPh$_2$[70] to (silox)$_3$Ta (**2**) at −78 °C, as indicated in eq 13. Deoxygenation of ketene

$$\underset{\mathbf{2}}{(\text{silox})_3\text{Ta}} + \text{Ph}_2\text{C}{=}\text{C}{=}\text{O} \xrightarrow[-78\ ^\circ\text{C}]{\text{hexane}} \underset{\mathbf{7}}{(\text{silox})_3\text{Ta}(\text{–O–C}{=}\text{CPh}_2)} \quad (13)$$

adduct (**7**) was achieved after extended thermolysis in benzene (8 h) at 155 °C. Oxo **3** was produced in virtually quantitative yield (^{1}H NMR) concomitant with PhC≡CPh (eq 14); it is

$$\mathbf{7} \xrightarrow[8\ \text{h}]{155\ ^\circ\text{C}} \underset{\mathbf{3}}{(\text{silox})_3\text{Ta}{=}\text{O}} + \text{PhC}{\equiv}\text{CPh} \quad (14)$$

possible that the latter was formed via rearrangement of the vinylidene, Ph$_2$C=C:, generated in the oxygen abstraction step.[20–22] Baldwin et al.[71] prepared similar diphenylketene adducts of trialkyl phosphites that display analogous deoxygenation reactions, exemplifying the common chemistry often observed for groups 5 and 15.

Attempts to scavenge transient vinylidene (silox)$_3$Ta=C=C: (**2**-C$_2$) have thus far been thwarted by various factors. The fragment molecular orbital diagram of the hypothetical

(69) (a) Casey, C. P.; O'Connor, J. M. *J. Am. Chem. Soc.* **1983**, *105*, 2919–2920. (b) Meinhart, J. D.; Santarsiero, B. D.; Grubbs, R. H. *Ibid.* **1986**, *108*, 3318–3323, and references therein.

(70) Ainsworth, C.; Chem, F.; Kuo, Y.-N. *J. Organomet. Chem.* **1972**, *46*, 59–71.

(71) (a) Baldwin, J. E.; Swallow, J. C. *J. Org. Chem.* **1970**, *35*, 3583–3584. (b) Mukaiyama, T.; Nambu, H.; Okamoto, M. *Ibid.* **1962**, *27*, 3651–3654.

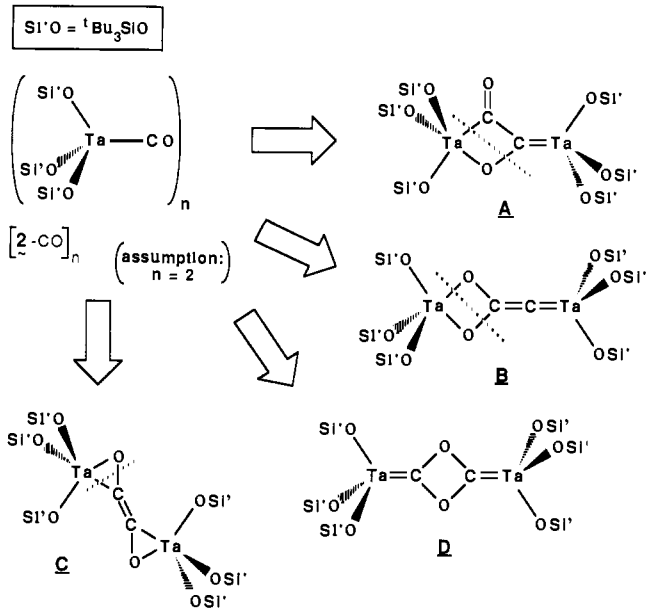

Figure 6. Possible structures of the red precipitate, $[(silox)_3TaCO]_n$ ($[2\text{-}CO]_n$, $n = 2$).

Scheme V

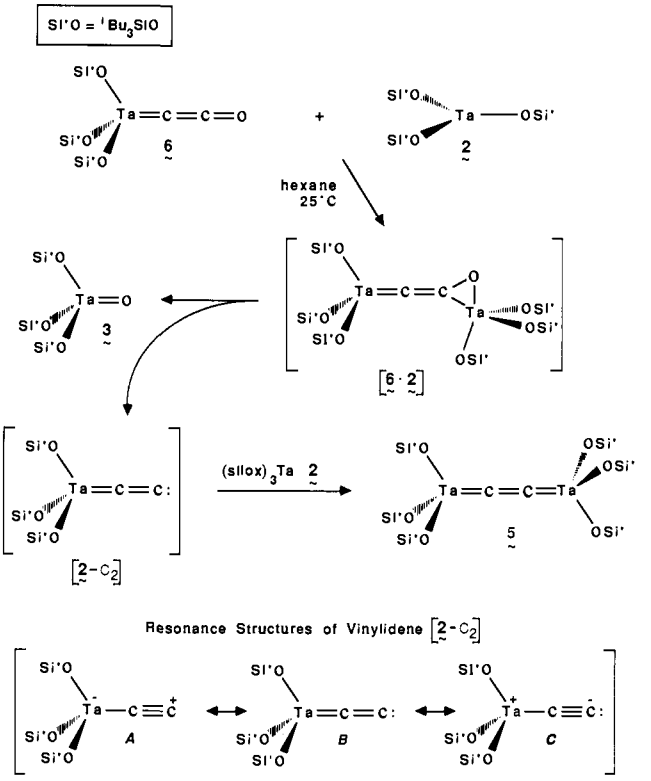

$(HO)_3Ta{=}C{=}C$: vinylidene in Figure 7 provides some rationale for the difficulties faced in trapping **2**-C_2. Vinylidenes and carbenes may be scavenged by electrophilic and nucleophilic agents depending on their electronic nature.[72,73] As the diagram illustrates, the $1a_1$ HOMO is quite low in energy, suggesting that a strong electrophile would be needed to attack this "lone pair" on the β-carbon. Unfortunately, electron-withdrawing substituents residing on olefinic and other likely electrophilic traps are subject

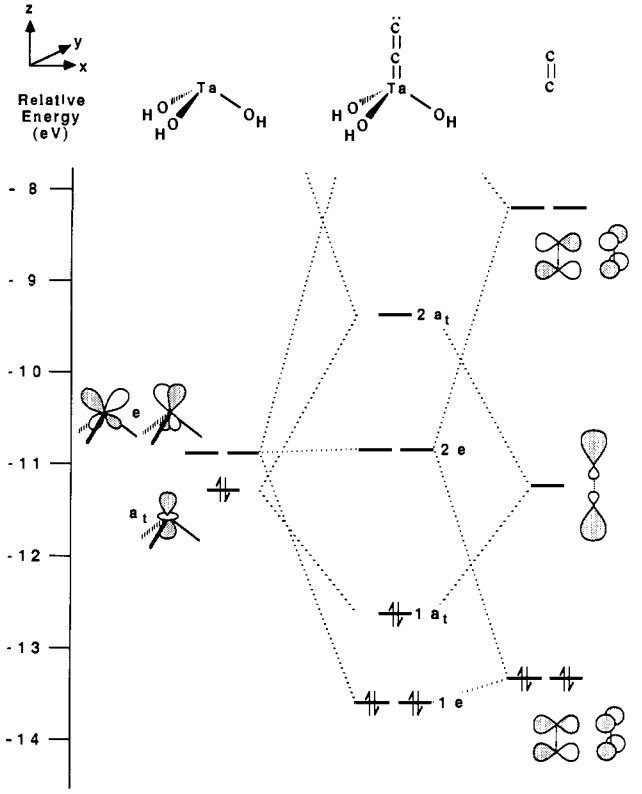

Figure 7. Truncated molecular orbital diagram of $(HO)_3Ta{=}C{=}C$: (**2'**-C_2), a model of the proposed intermediate vinylidene, $(silox)_3Ta{=}C{=}C$: (**2**-C_2).

to attack by the deoxygenating agent, $(silox)_3Ta$ (**2**). Reagents compatible with **2**, such as isobutylene, tetramethylethylene, and trialkylsilanes (e.g., neat Et_3SiH), proved ineffective, presumably due to electronic and steric factors. Nucleophilic scavengers[73] face severe steric problems because of the degenerate π-type, 2e LUMOs. Any nucleophile is required to approach the intermediate perpendicular to the TaCC axis, where it can be effectively blocked by the three silox groups. If steric considerations were not so important, an attack by a Nu: at either the Ta or β-carbon would be plausible, whereas C_α is basically a node. Consistent with these arguments, attempts to scavenge **2**-C_2 with compatible phosphines and other nucleophiles, such as electron-rich olefins, were unsuccessful.

A second electrophilic orbital is the $2a_1$, essentially a σ acceptor extending out from C_β. An attack by Nu: at the β-carbon appears unlikely because $2a_1$ is somewhat high in energy and a $4e^-$ repulsion problem would result as a consequence of an interaction with the filled $1a_1$ orbital. However, if the trapping agent possessed orbitals of π symmetry, the 2e set could be lowered concomitant with σ-bond formation; if the resulting π orbitals were populated rather than the new σ orbital, the $4e^-$ repulsion problem would be obviated. The latter argument reveals why $(silox)_3Ta$ (**2**) is such an effective scavenger of the vinylidene **2**-C_2. A $(silox)_3Ta$ fragment is an exceptional nucleophile in terms of the filled d_{z^2} orbital's energetic match with the high-energy $2a_1$ acceptor of **2**-C_2. In addition, relatively low-lying d_{xz} and d_{yz} orbitals can strongly interact with the 2e set of **2**-C_2, becoming the half-filled e_g level (HOMO) in $[(silox)_3Ta]_2(\mu\text{-}C_2)$ (**5**; see Figure 2). In essence, the vinylidene **2**-C_2 interacts with $(silox)_3Ta$ (**2**) in a fashion analogous to carbon monoxide (vide supra) and a similar case for strong binding can be proposed. The $1a_1$ orbital of **2**-C_2 is similar in energy to the carbon-based σ orbital of CO and the 2e set is related to the π^* orbitals of CO, except that they are energetically much lower and therefore subject to greater interaction with the relevant d orbitals of **2**.

At the bottom of Scheme V is a depiction of the resonance structures contributing to **2**-C_2. Given the electropositive character of Ta, structure C, with a positive charge on Ta and negative

(72) Kobrick, G.; Buck, P. In *Chemistry of Acetylenes*; Viehe, H. G., Ed.; Marcel Dekker: New York, 1969, p 99.

(73) Good nucleophiles have proven to be efficient traps of acyls and silaacyls. See: (a) Moloy, K. G.; Fagan, P. J.; Manriquez, J. M.; Marks, T. J. *J. Am. Chem. Soc.* **1986**, *108*, 56–67. (b) Bonnesen, P. V.; Yau, P. K. L.; Hersh, W. H. *Organometallics* **1987**, *6*, 1587–1590. (c) Arnold, J.; Tilley, T. D.; Rheingold, A. L.; Geib, S. J.; Arif, A. M. *J. Am. Chem. Soc.* **1989**, *111*, 149–164.

Scheme VI. Proposed Mechanism of Carbon Monoxide Cleavage

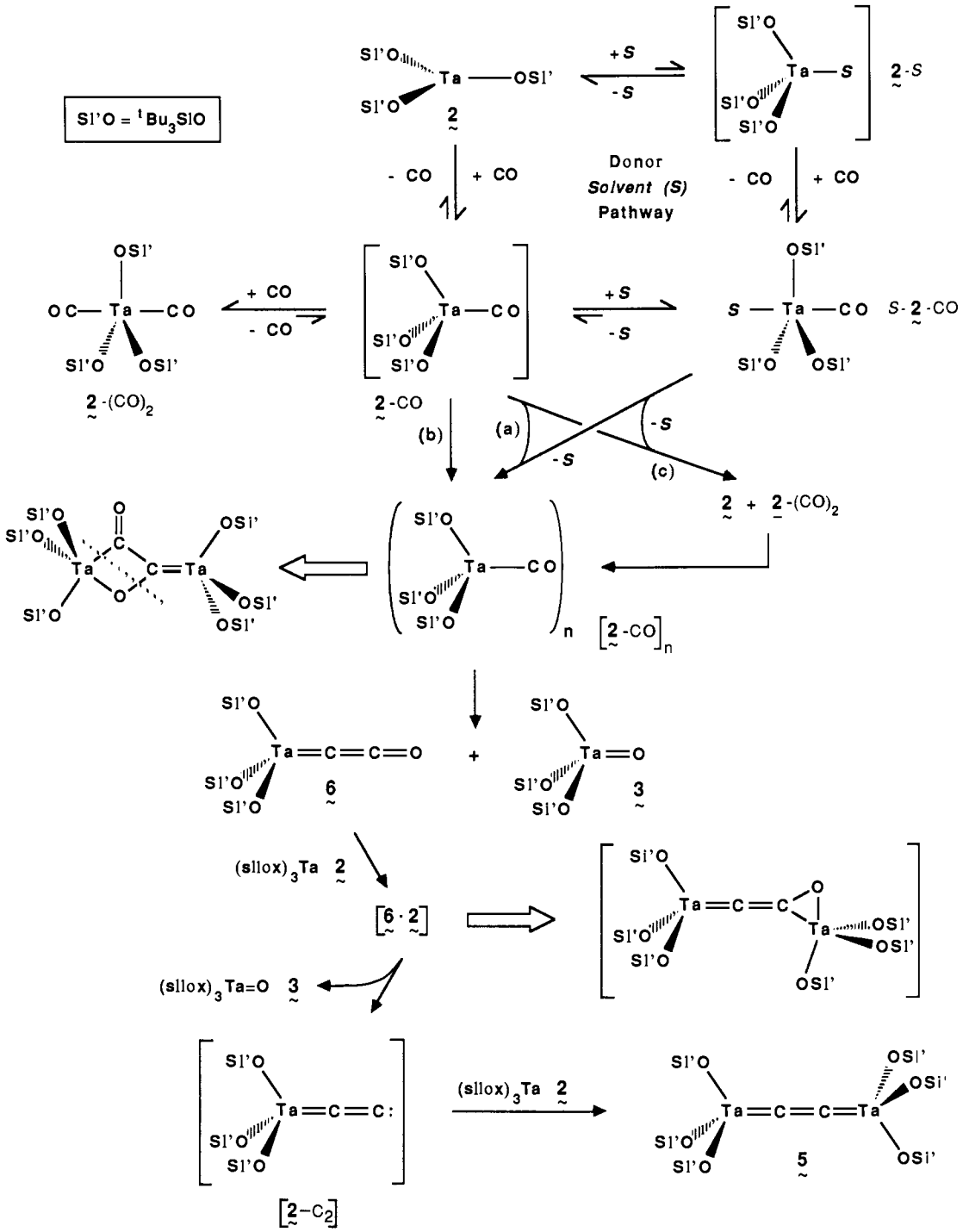

charge on C_β, must clearly be an important contributor. Here the similarity between **2**-C_2 and the valence bond representations of carbon monoxide as either :O=C: (B) or $^+$:O≡C:$^-$ (C) are readily apparent. Even resonance contributor A, considered somewhat unappealing since the formal negative charge resides on Ta, is interesting because it suggests that the vinylidene may be electrophilic at the β-carbon. This rationalization is comparable to the above discussion based on the molecular orbital diagram, where attack at the $2a_1$ molecular orbital by (silox)$_3$Ta (**2**) might be expected. In summary, both methods provide a rationalization why **2** is such an effective trap for the transient vinylidene, whereas conventional scavengers lack the specific, energetically matched σ- and π-electronic constituents necessary to interact with **2**-C_2 along the TaCC axis.

Mechanism Summary. From variable temperature, pressure, and mechanistic studies, the interrelationship of [(silox)$_3$Ta]$_2$(μ-C_2) (**5**) to the ketenylidene, (silox)$_3$TaCCO (**6**), can be summarized according to eq 15. The most plausible overall mechanism for

$$\underset{\mathbf{2}}{(\text{silox})_3\text{Ta}} \xrightarrow{(0.5+x)\text{CO}} 0.5\underset{\mathbf{3}}{(\text{silox})_3\text{Ta=O}} + x\underset{\mathbf{6}}{(\text{silox})_3\text{TaCCO}} + (0.5-x)/2\underset{\mathbf{5}}{[(\text{silox})_3\text{Ta}]_2(\mu\text{-}C_2)} \quad (15)$$

the formation of dicarbide (**5**), essentially a compilation of the previous schemes, is delineated in Scheme VI. Critical steps in the sequence are as follows: (1) (silox)$_3$Ta (**2**) binds CO to form an unstable, pseudotetrahedral, presumably paramagnetic adduct, (silox)$_3$TaCO (**2**-CO); (2) in donor solvents, **2**-CO is trapped and stabilized by the solvent (−78 °C) as (silox)$_3$*S*TaCO (*S*-**2**-CO); (3) either dimerization of **2**-CO (b), aggregation of *S*-**2**-CO and equilibrium amounts of **2**-CO (a), or disproportionation of **2**-CO to **2** and **2**-(CO)$_2$, which then quickly recombine (c), generates

a red precipitate (−78 − (−50 °C)), designated as $[(silox)_3TaCO]_n$ ($[\mathbf{2}\text{-CO}]_n$, $n = 2$); (4) either (b) or (c) leads to $[\mathbf{2}\text{-CO}]_n$ in non-donor solvents; (5) degradation of $[\mathbf{2}\text{-CO}]_n$, possibly through cleavage of the four-membered ring shown (~5 °C), produces the ketenylidene, $(silox)_3Ta{=}C{=}C{=}O$ (**6**) and the oxo, $(silox)_3Ta{=}O$ (**3**); (6) another $(silox)_3Ta$ (**2**) then deoxygenates ketenylidene **6** (~5 °C), probably via intermediate adduct $(silox)_3Ta{=}C{=}\overline{C{-}O{-}Ta(silox)_3}$ (**6**·**2**), to afford oxo **3** and a transient vinylidene, $(silox)_3Ta{=}C{=}C$: (**2**-C_2), that electronically resembles CO; (7) in the dicarbide-forming final step, a final $(silox)_3Ta$ (**2**) unit scavenges the vinylidene (**2**-C_2), resulting in $[(silox)_3Ta]_2(\mu\text{-}C_2)$ (**5**). The original observation that only dicarbide (**5**) was formed upon carbonylation of **2** in benzene was a consequence of the reaction conditions (eq 5). At 25 °C, formation of the red precipitate, $[\mathbf{2}\text{-CO}]_n$ is swift, but the complex quickly decomposes to give ketenylidene **6**. Under conditions of variable CO pressure (0.1–1.0 atm), **2** deoxygenates **6** and caps the resulting vinylidene, $(silox)_3Ta{=}C{=}C$: (**2**-C_2), faster than it is scavenged by CO. It is likely that the rate of CO dissolution at 25 °C is slow relative to this sequence of reactions.

Concluding Remarks

Two properties possessed by $(silox)_3Ta$ (**2**) appear to govern its ability to sever the C–O bond in carbon monoxide. The d^2 Ta(III) metal center is an extremely effective reductant, one capable of cleaving numerous C–X (X = O, S, halide, etc.) bonds.[74] A strong reducing ability of the metal is a necessary feature, since the formation of carbide (C^{4-}) or dicarbide ($^1/_2C_2^{4-}$) and oxide (O^{2-}) from CO requires six or four electrons, yet this property alone is not sufficient to induce CO scission. At critical stages in the carbonylation of $(silox)_3Ta$ (**2**) to provide dicarbide, $[(silox)_3Ta]_2(\mu\text{-}C_2)$ (**5**), certain intermediates, including oxophilic **2**, act as potent electrophiles. These characteristics enable attack of the carbon monoxide, in whatever bound form it exists, at both ends of the small molecule. As electron density is being transferred to carbon by a d^2 tantalum center, removal of electron density, via loss of O^{2-} to give $(silox)_3Ta{=}O$ (**3**), occurs at a cooperating tantalum. Presumably, the initial, formal reduction of the carbon half of CO occurs via the coupling of two carbonyls in the formation of $[(silox)_3TaCO]_n$ ($[\mathbf{2}\text{-CO}]_n$), the red precipitate. Related couplings of CO with carbynes,[75] alkylidenes,[76] and alkyls (migratory insertion)[77] as well as the formation of other two-carbon fragments[13,78] provide precedent. In reviewing the ditungsten-[26] and samarium-based[27] systems that have been shown to sever the CO triple bond, in addition to those that couple two CO molecules,[31,32] the combination of an electron-donating (i.e., π-back-bonding), yet electrophilic metal center(s) appears crucial.

Although it is difficult to assess the overall thermodynamics of dicarbide (**5**) formation, one important factor is the accompanying production of the tantalum oxo unit in **3**. Other contributions from the dicarbide, including generation of a C=C double bond and robust Ta=C fragments, are certainly significant. A strengthening of Ta(silox) bonds as **2** is oxidized to Ta(V) species is presumed to be a relatively minor factor, especially since it must be partially offset by the increased steric factors present in the four-coordinate carbonylation products. The influence of oxo (**3**) production on the thermodynamics of CO scission must also be pronounced when ketenylidene, $(silox)_3Ta{=}C{=}C{=}O$ (**6**),

Scheme VII

Possible Carbon Monoxide Dissociation Pathways

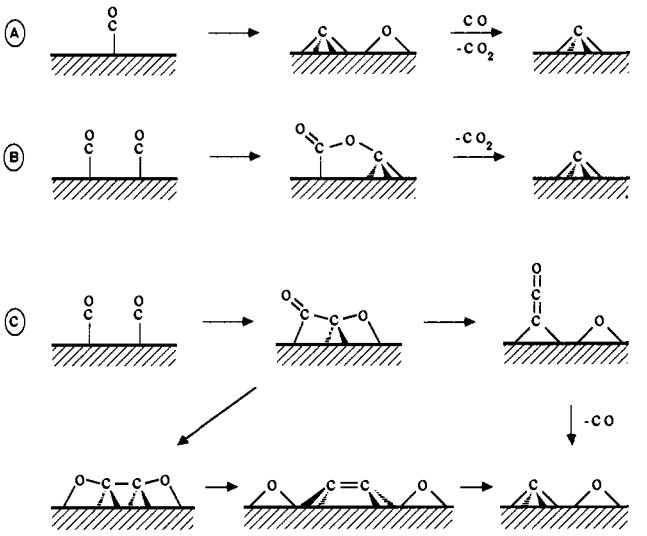

results from carbonylation (~1 atm) of **2**. In this instance, 0.5 equiv of CO/Ta has been cleaved, while another 0.5 equiv has been reduced in bond order via incorporation into the CCO ligand.

Claims of a significant relationship between metal carbonyl cluster carbide formation and the dissociative adsorption of CO on heterogeneous F–T catalysts have been expounded upon.[7,8] Some elaboration is required to assess the relationship between heterogeneous surfaces and cleavage of CO as mediated by $(silox)_3Ta$ (**2**), since tantalum is not a typical component of F–T catalysts. Silica supports of common F–T catalysts are modeled by the ancillary siloxide ligands that effect a more electrophilic metal center. It is important to recognize that the extremely electropositive character of early metals leads to the ready formation of metal–oxygen bonds,[18-22,26,27] hence the unusual, low-temperature cleavage of CO by **2** may be a consequence of $(silox)_3Ta{=}O$ (**3**) formation. The thermodynamics of CO dissociative adsorption on various metal surfaces have been analyzed by Benziger, whose calculations show that the exothermicity of the process increases from group 8 to group 4.[6,79,80] For groups 4 and 5, $\Delta H_{diss}(CO)$ also becomes more exothermic down each column. These trends stem from a general decrease in the heats of formation of the various carbides and oxides across a particular row. Clearly, an important assumption must be made; the mild CO reduction herein can be considered an appropriate model for the heterogeneous process if the overall exothermicity serves to lower kinetic barriers with individual steps, and that these steps are akin to those occurring on typical F–T surfaces.

If one accepts the above premise that early metal complexes exhibit reactivity commensurate with F–T systems that operate at substantially higher temperatures and pressures,[1-4] some important conclusions may be drawn from the unusual chemistry portrayed herein. First, it is evident that only two metal centers are necessary for the cleavage of 1 equiv of CO, since only two tantalums are involved in the formation of ketenylidene $(silox)_3Ta{=}C{=}C{=}O$ (**6**) and oxo $(silox)_3Ta{=}O$ (**3**; eq 8). Only three tantalum units are needed to sever two CO molecules if one considers the proposed vinylidene, $(silox)_3Ta{=}C{=}C$: (**2**-C_2), which contains a C_2^{2-} dicarbide ligand, as the primary cleavage product; a fourth is needed to form the ultimate dicarbide complex, $[(silox)_3Ta]_2(\mu\text{-}C_2)$ (**5**). These conclusions are straightforwardly obtained from stoichiometry, noting that **2** is a $2e^-$ reductant. Even if CO had been converted to a carbido (C^{4-}) ligand, only three tantalum units would have been required. The relevance to heterogeneous systems is apparent. Although an ensemble of about

(74) Neithamer, D. R. Ph.D. Thesis, Cornell University, 1989.
(75) (a) Birdwhistell, K. R.; Tonker, T. L.; Templeton, J. L. *J. Am. Chem. Soc.* **1985**, *107*, 4474–4483. (b) Mayr, A.; McDermott, G. A.; Dorries, A. M.; Van Engen, D. *Organometallics* **1987**, *6*, 1503–1508, and references therein.
(76) (a) Morrison, E. D.; Steinmetz, G. R.; Geoffroy, G. L.; Fultz, W. C.; Rheingold, A. L. *J. Am. Chem. Soc.* **1984**, *106*, 4783–4789. (b) Morrison, E. D.; Geoffroy, G. L. *Ibid.* **1985**, *107*, 3541–3545. (c) Bassner, S. L.; Morrison, E. D.; Geoffroy, G. L. *Ibid.* **1986**, *108*, 5358–5359, and references therein.
(77) Collman, J. P.; Hegedus, L. S.; Norton, J. R.; Finke, R. G. *Principles and Applications of Organotransition Metal Chemistry*; University Science Books: Mill Valley, CA, 1987; pp 356–376.
(78) Wilker, C. N.; Hoffmann, R.; Eisenstein, O. *Nouv. J. Chim.* **1983**, *7*, 535.
(79) Benziger, J. B. *Appl. Surf. Sci.* **1980**, *6*, 105–121.
(80) For a recent experimental study involving CO dissociation on Cr(110), see: Shinn, N. D.; Madey, T. E. *J. Chem. Phys.* **1985**, *83*, 5928–5944.

five atoms is depicted in a typical portrayal of the dissociative adsorption of CO on surfaces, the only requirements are either six (to C^{4-} and O^{2-}) or four electrons (to $^1/_2C_2^{4-}$ and O^{2-}), and whatever number of metals that can supply this quantity. Additionally, a Lewis acidic site is useful in accelerating the cleavage, but the same metal can act in both capacities.

The chemistry herein also suggests additional pathways for the dissociation of carbon monoxide (Scheme VII). Illustrated in A is the straightforward dissociative adsorption of CO to give surface carbide, C_s, and oxide, O_s, that is abstracted by an additional CO to generate CO_2, a process known as the Boudouard disproportionation of CO. Consider B, where two surface carbonyls, $(CO)_s$, interact directly to form C_s and CO_2, a hypothetical pathway that circumvents the necessity to dissociatively adsorb CO. Note that CO could catalyze the formation of surface carbide in this manner if the CO_2 produced was deoxygenated by the surface to give O_s and $(CO)_s$ or CO. The surface mechanisms depicted in C appear quite complicated, but they are merely adaptations and variations of the homogeneous processes delineated above. Formation of a surface CCO group, perhaps analogous to those of trimetallic clusters,[38-41,44] followed by decarbonylation represents one possibility. Another model is illustrated by the coupling of CO units[30-32] and the subsequent deoxygenation of the $(OCCO)_s$ fragment to give a dicarbide. Given the reactivity described herein, complementary W-[26] and Sm-based[27] studies, and the ready formation of carbonyl cluster carbonyls,[7] mechanisms addressing the dissociation of carbon monoxide may require that $(CO)_s$ units interact directly. In conclusion, while the dissociative adsorption of carbon monoxide is an experimentally verified occurrence, intriguing questions regarding the mechanism(s) by which adsorbed CO cleaves to give surface carbide and oxide remain.

Experimental Section

General Considerations. All manipulations were performed with use of either glovebox or high vacuum line techniques. Ethereal and hydrocarbon solvents were distilled under nitrogen from purple benzophenone ketyl and vacuum transferred from the same prior to use. Benzene-d_6 was dried over activated 4-Å molecular sieves, vacuum transferred, and stored under N_2; THF-d_8 was dried over sodium benzophenone ketyl. Argon and hydrogen were passed over MnO on vermiculite and activated 4-Å sieves. Carbon monoxide and oxygen (Matheson) were used as received. Tantalum pentachloride (Alfa) was sublimed at 115 °C (10^{-4} Torr) prior to use. Sodium tri-*tert*-butyl siloxide (Na(silox))[16] and diphenylketene[70] were prepared via literature procedures.

NMR spectra were obtained with Varian XL-200 (^{1}H) and XL-400 (^{1}H (VT), ^{13}C{^{1}H}, ^{29}Si{^{1}H}) spectrometers. Chemical shifts are reported relative to TMS (^{1}H, ^{29}Si{^{1}H}) or benzene-d_6 (^{1}H, δ 7.15; ^{13}C{^{1}H}, δ 128.00). Infrared spectra, including kinetics runs, were recorded on a Mattson FT-IR interfaced to a AT&T PC7300 computer. For variable-temperature studies, a Specac 21000 variable-temperature cell with manual temperature controller and flow-through adapter was utilized. UV–vis spectra were recorded on Hewlett-Packard 8451A (200–800-nm) and Cary 17D (400–3000-nm) spectrometers. Melting points were acquired with a Meltemp apparatus and are reported uncorrected. Molecular weights were obtained with a home-built device for benzene cryoscopy. Analyses were performed by Analytische Laboratorien, Elbach, West Germany.

Procedures. 1. (silox)$_3$TaCl$_2$ (1). To a flask containing $TaCl_5$ (3.95 g, 11.0 mmol), and Na(silox) (7.88 g, 33.0 mmol, 3.00 equiv) was distilled 120 mL of toluene. The mixture was warmed to 25 °C and allowed to react under Ar for 9 h followed by 15 h at reflux. After the solution was concentrated to dryness, the residue was dissolved in hexanes and filtered to give a pale yellow solution and a gelatinous, white solid. The solid was repeatedly washed with 30-mL portions of hexanes until no soluble material remained. Reduction of the volume to 50 mL and cooling to −78 °C resulted in colorless crystals that were collected by filtration and dried in vacuo to yield a white powder (5.76 g). Resubmission of the filtrate for a second crop gave another 2.13 g (80% total yield): ^{1}H NMR (C_6D_6) δ 1.34; ^{13}C{^{1}H} NMR (C_6D_6) δ 30.63 (C(*C*H$_3$)$_3$), 24.93 (*C*(CH$_3$)$_3$). Anal. Calcd for $C_{36}H_{81}O_3Si_3Cl_2Ta$: C, 48.14; H, 9.09. Found: C, 47.99; H, 8.93.

2. (silox)$_3$Ta (2). To a flask containing (silox)$_3$TaCl$_2$ (**1**; 7.00 g, 7.79 mmol) and 0.9% Na/Hg (79.9 g, 31.2 mmol (Na)) was distilled 120 mL of THF at −78 °C. While the solution was warmed to 25 °C and stirred for 2 h, a color change from colorless to purple, to blue, and then to blue-green was observed. The THF was removed under vacuum and as much Hg decanted as possible. The residue was dissolved in hexanes and filtered, giving a blue-green solution and a blue-gray solid. The solid was repeatedly washed with 30-mL portions of hexanes until devoid of any blue color. Concentration of the solution to 40 mL, cooling to −78 °C, and filtration yielded blue crystals. The crystals were washed once with cold hexanes and then dried in vacuo (4.77 g, 74%). Variable yields (60–85%) have been obtained depending on the purity of **1** and the length of the reaction time (the yield diminishes beyond 2 h). Complex **2** is unstable with respect to cyclometalation,[28] but can be kept for months at −20 °C: ^{1}H NMR (C_6D_6) δ 1.32; ^{13}C NMR (C_6D_6) δ 31.75 (C(*C*H$_3$)$_3$), 22.83 (*C*(CH$_3$)$_3$); ^{29}Si NMR (C_6D_6) δ 18.63; UV–vis 216 nm ($\epsilon \sim 6800$ M^{-1} cm^{-1}), 306 (12900), 350 (1200), 364 (2400), 394 (1100), 570 (25), 612 (36), 680 (25), 840 (25), 928 (33); M_r calcd 827, found 800.

3. (silox)$_3$Ta=O (3) (from 2 + Excess O$_2$). A flask containing (silox)$_3$Ta (**2**) (300 mg, 0.363 mmol) and 10 mL of benzene at 25 °C was exposed to 1 atm O_2. The blue solution immediately bleached and ultimately turned pale orange. After removal of the benzene and addition of 10 mL of Et_2O, the solution was filtered. Crystallization from ~1 mL of Et_2O afforded 130 mg (43%) of off-white **3**: ^{1}H NMR (C_6D_6) δ 1.27; (THF-d_8) 1.23; ^{13}C{^{1}H} NMR (C_6H_6) δ 30.54 (C(*C*H$_3$)$_3$), 23.71 (*C*(CH$_3$)$_3$); IR (Nujol) ν(Ta=O) = 905 cm^{-1}; M_r calcd 842, found 800. Anal. Calcd for $C_{36}H_{81}O_4Si_3Ta$: C, 51.28; H, 9.68. Found: C, 51.13; H, 9.52.

4. (silox)$_3$TaH$_2$ (4). A flask containing (silox)$_3$Ta (**2**; 300 mg, 0.363 mmol) and 10 mL of benzene at 25 °C was exposed to 1 atm H_2. The blue color discharged within 1 h. After removal of the benzene and addition of 10 mL of hexanes, the solution was filtered. Crystallization from ~5 mL of hexanes afforded 240 mg (80%) of colorless **4**: ^{1}H NMR (C_6D_6) δ 1.26 (s, CH$_3$, 81 H), 21.99 (s, TaH$_2$, 2 H); ^{13}C{^{1}H} NMR (C_6D_6) δ 30.49 (C(*C*H$_3$)$_3$), 23.37 (*C*(CH$_3$)$_3$); ^{29}Si{^{1}H} NMR (C_6D_6) δ 15.29; IR (Nujol) ν(TaH$_2$/D$_2$) = 1725/1250 cm^{-1}, δ(TaH$_2$/D$_2$) = 750/570 cm^{-1}; UV–vis 218 nm ($\epsilon \sim 5100$ M^{-1} cm^{-1}), 278 (4400). Anal. Calcd for $C_{36}H_{83}O_3Si_3Ta$: C, 52.14; H, 10.09. Found: C, 51.90; H, 10.05.

5. [(silox)$_3$Ta]$_2$(μ-C$_2$) (5) and (silox)$_3$Ta=O (3). a. To a flask containing (silox)$_3$Ta (**2**; 500 mg, 0.605 mmol) was added 20 mL of C_6H_6 at −78 °C. The flask was warmed to 25 °C to give a clear blue solution and then opened to a calibrated gas bulb containing CO (0.604 mmol, 1.00 equiv). The initial blue color was immediately discharged to give a red precipitate. After stirring at 25 °C for 30 min, the volatiles were passed through three LN_2 traps and the noncondensible gas collected with a Toepler pump (0.32 mmol, 0.53 equiv). The red residue was slurried in 15 mL of hexanes and filtered to separate the brick red solid (**5**) from a pink solution.

The solid was washed with three 3-mL portions of hexanes, dried in vacuo, and collected to give 255 mg of material. The solid was further purified by rapid stirring in warm hexane followed by filtration (235 mg, 46% based on Ta): ^{1}H NMR (C_6D_6) δ 2.03 ($\nu_{1/2} \sim 10$ Hz); (THF-d_8) 1.88 ($\nu_{1/2} \sim 10$ Hz); ^{13}C{^{1}H} NMR (THF-d_8, 40 °C) δ 53.45 (*C*(CH$_3$)$_3$), 44.50 (C(*C*H$_3$)$_3$), μ-$^{13}C_2$ not located; IR (Nujol) (**5**, μ-C$_2$) 709 cm^{-1}, (**5**-C^{13}C, μ-C^{13}C) 695, (**5**-$^{13}C_2$, μ-$^{13}C_2$) 682; Raman **5**/**5**-$^{13}C_2$ ν(C=C/^{13}C=^{13}C) = 1617/1549 cm^{-1}; UV–vis 214 nm ($\epsilon \sim 15000$ M^{-1} cm^{-1}), 256 (9000), 280 (11000), 310 (52000), 350–600 (3000–6000). Anal. Calcd for $C_{74}H_{162}O_6Si_6Ta_2$: C, 52.95; H, 9.73. Found: C, 52.73; H, 9.58.

The filtrate was concentrated to dryness to give 230 mg (47% based on Ta) of pink solid. Recrystallization from Et_2O gave 150 mg of pale pink powder. Sublimation (190 °C (10^{-4} Torr)) of the powder gave analytically pure **3** (70 mg, 27%).

b. Hydrolysis of 5. An NMR tube sealed to a 14/20 joint was charged with 25 mg of [(silox)$_3$Ta]$_2$(μ-C$_2$) (0.015 mmol) and ~0.5 mL of THF-d_8. The tube was attached to a gas bulb (90.4 mL) and the resulting solution freeze–pump–thaw degassed three times. An excess of H_2O (five 10-Torr portions, 0.24 mmol) was condensed at 77 K and the tube sealed with a torch. After warming to 25 °C, the sample was placed in a 110 °C bath for 15 h after which a suspended white precipitate and a pale yellow-orange solution remained. ^{1}H NMR showed (silox)H and ethylene as the only observable products.

6. (silox)$_3$Ta=C=C=O (6) and (silox)$_3$Ta=O (3). a. To a 50-mL glass bomb reactor charged with (silox)$_3$Ta (255 mg, 0.309 mmol) was added 10 mL of toluene at −78 °C. The bomb was opened to a calibrated Toepler manifold containing CO (305 Torr, 3.08 mmol), immediately discharging the blue color to give a red insoluble precipitate. After stirring the solution for 1 h, the bomb was cooled to 77 K and sealed under 252 Torr CO. The solution was then allowed to warm to room temperature with stirring during which the red solid was consumed (between 5 and 10 °C) to give a pale orange solution and a minute amount of white precipitate. The volatiles were removed via vacuum transfer through three LN_2 traps and the excess gas collected with the

Toepler pump (271 Torr, 2.80 mmol) indicating an uptake of 0.91 equiv of CO. The residue was dissolved in hexanes and filtered to remove the white precipitate. Reduction of the volume to 5 mL, cooling to −78 °C, filtering, and drying in vacuo afforded a 1.1:1 off-white mixture of **3** and **6** (167 mg, 54%). Efforts to separate the mixture by fractional crystallization were unsuccessful. If the solvent is simply removed, the yield of crude **3** plus **6** is ~90%: ^{1}H NMR (**6**, C_6D_6) δ 1.25; (THF-d_8) 1.25; $^{13}C\{^1H\}$ NMR (C_6D_6) δ 142.51 (d, J_{CC} = 100 Hz, *C*CO), 135.96 (br d, J_{CC} = 100 Hz, *C*CO), 30.42 (C(*C*H$_3$)$_3$), 23.64 (*C*(CH$_3$)$_3$); IR (C_6H_{12}) $\nu(^{12}C^{12}CO)$ = 2076, $\nu(^{13}C^{12}CO)$ = 2065, $\nu(^{12}C^{13}CO)$ = 2022, $\nu(^{13}C^{13}CO)$ = 2011 cm^{-1}.

b. 6 and 3 from [(silox)$_3$Ta]$_2$(μ-C$_2$) (5) and O$_2$. A 25-mL flask was charged with 50 mg of [(silox)$_3$Ta]$_2$(μ-C$_2$) (0.03 mmol) and attached to a 180° needle valve. Pentane (~15 mL) was vacuum transferred into the flask at −78 °C, the flask was warmed to 25 °C, and the slurry was exposed to 1 atm O_2 with vigorous stirring. After 30 min the red precipitate was completely discharged to yield a clear, pale yellow solution. Concentration to dryness led to an off-white powder. ^{1}H NMR showed a 1.1:1 ratio of **3** to **6** (~90%).

c. 2,5-Dimethyltetrahydrofuran Solvent. A flask charged with **2** (47 mg, 0.057 mmol) and 2 mL of 2,5-Me$_2$-THF was exposed to 100 Torr CO (2.7 mmol) at −78 °C. The red precipitate was observed to form instantly, and after being stirred for 1 h, was allowed to settle out. On warming to 25 °C, the solid dissolved to give a peach solution. Upon removal of solvent, the residue showed a 1.15:1 ratio of **3** to **6**.

d. 6-$^{13}C_2$ + 6 Crossover to 5-$^{13}C_2$ + 5. To a flask charged with an approximate 1:1 mixture of **3** and **6** (38 mg, 0.022 mmol **6**), a 1:1 mixture of **3** and **6**-$^{13}C_2$ (38 mg, 0.022 mmol **6**-$^{13}C_2$), and **2** (74 mg, 0.090 mmol) was added 10 mL of toluene at −78 °C. The solution was allowed to warm to 25 °C to generate dicarbide, which was isolated by filtration and washed three times (56 mg). An IR (Nujol) showed only two low-energy stretches at 711 (μ-C$_2$) and 687 (μ-$^{13}C_2$) cm^{-1}, indicative of **5** and **5**-$^{13}C_2$.

7. a. (silox)$_3$Ta(η^2-(O,C)OC=CPh$_2$) (7). To a flask containing (silox)$_3$Ta (376 mg, 0.455 mmol) and 15 mL of pentane at −78 °C was syringed under a vigorous Ar counterflow 4.40 mL of a 0.103 M diphenylketene/hexane stock solution (0.453 mmol, 1.00 equiv). A clear yellow solution was immediately observed. The reaction was allowed to warm to room temperature over a 3-h period and then cooled to −78 °C. Reduction of the solution volume to 3 mL, filtering, and cooling yielded microcrystals (185 mg, 40%): ^{1}H NMR (C_6D_6) δ 7.79 (d"t", *J* = 7.4 Hz, 2 H), 7.63 (d"t", *J* = 7.4 Hz, 2 H), 7.35–7.00 (m, 6 H), 1.21 (s, 81 H, silox); ^{13}C NMR (C_6D_{12}) δ 130.65 (d, $^1J_{CH}$ = 130.5 Hz), 127.99 (d, $^1J_{CH}$ = 127.8 Hz), 125.72 (d, $^1J_{CH}$ = 125.6 Hz), 30.93 (C(*C*H$_3$)$_3$), 23.97 (*C*(CH$_3$)$_3$), the four quaternary carbons could not be located. Anal. Calcd for $C_{50}H_{91}O_4Si_3Ta$: C, 58.79; H, 8.98. Found: C, 59.77; H, 9.01.

b. Thermolysis of 7. A 5-mm NMR tube sealed to a 14/20 joint was charged with 20 mg (0.019 mmol) of **7** and 0.5 mL of C_6D_6 and attached to a 180° needle valve. The solution was freeze–pump–thaw degassed three times. The tube was sealed with a torch and placed in a 155 °C bath for 8 h; **7** slowly disappeared as (silox)$_3$Ta=O (**3**) and PhC≡CPh grew in. The temperature was raised to 220 °C and after 1 h the reaction was complete. The tolane was correlated by NMR with an authentic sample.

8. (silox)$_3$(THF)TaCO (THF-2-CO). a. Synthesis and CO Uptake. A flask containing (silox)$_3$Ta (**2**; 250 mg, 0.302 mmol) and 25 mL of THF at −78 °C was exposed to CO (861 Torr, 0.907 mmol, 3.00 equiv) from a calibrated gas bulb (19.6 mL). A clear yellow solution, indicating the presence of THF-**2**-CO was immediately observed. After being stirred for 15 min, the solution was degassed with the Toepler pump and the gas collected in a 63-mL volume (144 Torr, 0.612 mmol). The gas was converted to CO_2 upon circulation over CuO (300 °C), thus indicating an uptake of 0.97 equiv of CO (0.295 mmol)/Ta. During the degassing, a continuous color change from clear yellow to orange occurred. After degassing, the solution was allowed to warm and copious precipitation of a red solid was observed at ~−50 °C. On warming to 25 °C, the solid dissolved (~5 °C) to give a pale peach solution. The solvent was removed and a ^{1}H NMR (C_6H_6) of the solid showed an approximate 1:1 mixture of **3** and **6**.

b. Curie Plot (δ vs 1/*T*) for (THF-2-CO). From −112 to −88 °C the weighted average of the two resonances were plotted vs 1/*T*. From −76 to −42 °C, the now clearly coalesced resonance was plotted vs 1/*T*. The plot was linear throughout (r^2 = 0.9998) and approaches 0 in the limit of $T \rightarrow \infty$.[59]

c. Coalescence of silox Resonances. A 5-mm NMR tube sealed to a 14/20 joint was charged with 15 mg (0.019 mmol) of **2** and attached to a 180° needle valve. THF-d_8 (~0.4 mL) was condensed into the tube and freeze–pump–thaw degassed twice. The tube was sealed with a torch under 60 Torr CO (~0.04 mmol, ~2 equiv) and kept frozen at 77 K. The sample was allowed to warm to −78 °C while completely immersed in a CO_2/acetone slush bath and completely mixed to form intermediate THF-**2**-CO. The tube was frozen in LN_2 and then placed in the 400-MHz NMR probe, which had previously been cooled to ~−80 °C. Once the sample thawed, the probe was cooled to −112 °C and data collection began. Points were collected at 2 °C intervals over the range −112 to −42 °C with a 90-s delay set between each point to allow for equilibration. Two transients were collected for each spectra, which consisted of two resonances (δ 12.4 ($\nu_{1/2}$ = 200 Hz); δ 7.7 ($\nu_{1/2}$ = 90 Hz) at −112 °C) in a 2:1 ratio which shift according to Curie behavior and coalescence at −80 (1) °C (k_{coal} = 1.4 (2) × 10^3 s^{-1}; $\Delta G^{\ddagger}$ = 8.4 (1) kcal/mol). The rate of coalescence was estimated by using the empirical formula described by Sandström[81] for an unequally populated site exchange: $k_a = 2\pi p_b(\Delta\nu)/x$ (p_b, population in site b, 0.333; Δν, chemical shift difference (Hz) at the low-temperature limit; x = 2.0823, an empirical parameter indicating a 2:1 site exchange). The chemical shift difference, Δν, was determined by extrapolating Curie plots of the two resonances (−112 to −88 °C) to the coalescence temperature (−80 °C).

To test for a coalescence process that would involve association of a second CO, four tubes were loaded with **2** and CO as described above. In tubes containing 1, 3, 8, and 17 equiv of CO, the coalescence temperature remained −80 °C; hence the equilibration of the silox resonances was independent of [CO]. To test for a coalescence process that would involve association of THF, mixtures of THF-d_8/methylcyclohexane-d_{14} were used. Measurements similar to those above indicated that the coalescence temperature remained −80 °C.

d. NMR Kinetics of THF-2-CO Disappearance. For a typical run, two 5-mm NMR tubes sealed to 14/20 joints were each charged with **2** (15 mg, 0.018 mmol) and THF-d_8 (0.60 mL, [Ta] = 3.0 × 10^{-2} M), the latter via graduated pipet. They were then attached to 180° needle valves, freeze–pump–thaw degassed three times, sealed with a torch under 60 Torr CO (~0.025 mmol), and kept frozen in LN_2. The samples were allowed to warm to −78 °C while completely immersed in a CO_2/acetone slush bath, then thoroughly mixed to form THF-**2**-CO, and then refrozen in LN_2.

The first tube was placed in the 400-MHz probe, which had previously been cooled to −80 °C. Once the sample thawed, the probe was warmed to −71 °C and data collection begun. At t = 0, the above paramagnetic resonances comprised 0.60 of the total spectrum integration, thus [THF-**2**-CO]$_0$ ≤ 1.8 × 10^{-2} M. This is the maximum concentration of THF-**2**-CO (yielding the minimum second-order rate constants), because any material that has precipitated is not included in the [Ta]$_{tot}$ obtained from integration. Some of the red precipitate, [(silox)$_3$TaCO]$_n$ ([**2**-CO]$_n$), was present in the NMR tubes prior to the start of each kinetics run, and thus the t = 0 s concentrations of THF-**2**-CO were somewhat less. After a 2-min equilibration period, 16 points were collected at 64-s intervals. Two transients were collected for each spectrum, which was integrated by using THF-d_7 as an internal standard. The integrals of the peaks were followed, leading to second-order disappearance of THF-**2**-CO ($k \geq$ 0.2 (1) M^{-1} s^{-1}) with r^2 = 0.996 (cf. first order, r^2 = 0.974). The second tube was similarly monitored at −63 °C: [THF-**2**-CO]$_0$ ≤ 1.5 × 10^{-2} M; 13 points at 64-s intervals. The second-order rate constant at −63 °C was found to be $k \geq$ 0.5 (1) M^{-1} s^{-1} (r^2 = 0.994; cf. first order, r^2 = 0.928).

e. IR of THF-2-CO. A 25-mL two-neck flask with a septum in one neck was charged with 40 mg of **2** (0.048 mmol) and attached to a 180° needle valve. THF (~12 mL) was vacuum distilled into the flask at −78 °C ([**2**] = ~4 × 10^{-3} M). On exposure to 100 Torr CO from the manifold (2.4 mmol), an immediate pale blue to yellow color change was observed. After stirring for 5 min, the solution was degassed and backfilled with 1 atm Ar. A 3-mL portion was withdrawn with a syringe cooled to −78 °C and the sample injected into the variable-temperature IR cell, which had previously been equilibrated to −77 °C. A single band in the CO stretching region was observed at 1840 cm^{-1}, which slowly disappeared with time. When ^{13}CO was used, the stretch was observed at 1796 cm^{-1} (ν_{calcd} = 1799 cm^{-1}).

f. IR Kinetics of THF-2-CO Disappearance. A 25-mL two-neck flask with a septum in one neck was charged with 30 mg of **2** (0.036 mmol) and attached to a 180° needle valve. By use of a graduated cylinder connected to a 180° needle valve, 10.0 mL of THF were measured out and vacuum transferred into the flask ([**2**] = 3.6 × 10^{-3} M). The solution was exposed at −78 °C to 1 atm CO from the manifold (18.4 mmol) and stirred for 10 min. The flask was evacuated for 8 min and then backfilled with Ar. A 4-mL portion was withdrawn with a syringe cooled to −78 °C and the contents injected into the variable-temperature IR cell, which had previously been equilibrated to −72 °C. Two bands in the CO stretching region were observed at 1870 and 1840 cm^{-1} in an ~2:6 ratio. Over time, the 1870-cm^{-1} stretch remained constant while the 1840-cm^{-1} band decreased in intensity. The disappearance of the 1840-cm^{-1} peak

(81) Sandström, J. *Dynamic NMR Spectroscopy*; Academic Press: New York, 1982; p 81.

(−72 °C, nine points, 2.9 half-lives, $k \geq 0.4$ (0.1) M^{-1} s^{-1}, $r^2 = 0.992$) followed second-order kinetics.

g. THF-2-CO and THF-2-^{13}CO Crossover. Two three-neck flasks were each charged with 57 mg of **2** (0.069 mmol) and capped with a glass stopper and a septum. THF (50 mL) was distilled into each flask at −78 °C. The first flask was opened to a manifold containing 66 Torr ^{13}CO (1.6 mmol) and the other flask exposed to 95 Torr ^{12}CO (2.3 mmol). Clear yellow solutions were immediately observed in both flasks. After stirring for 45 min, the solutions were separately degassed and exposed to 1 atm Ar. The contents of the flasks were then combined via a cannula that was swabbed with dry ice/acetone. After 10 min, the clear yellow-orange solution was allowed to warm to 25 °C for 3 h. During this period the red precipitate formed and then disappeared. The resulting pale orange solution was concentrated to dryness. The IR (C_6H_{12}) spectrum of the solid showed a 33:26:16:25 ratio of **6**:(**6**-^{13}CC):**6**-C^{13}C:**6**-$^{13}C_2$. If a completely random crossover occurred, an approximate 30:25:25:20 ratio would be observed for 90% ^{13}CO enrichment; hence, this experiment essentially shows a statistical distribution of the label. The slight discrepancy may be due to some dimerization during cannulation, which would increase the amount of isotopically pure ketenylidenes at the expense of the mixed ketenylidenes.

h. CO Exchange with THF-2-^{13}CO. To a flask charged with **2** (57 mg, 0.069 mmol) was added 25 mL of THF at −78 °C. The solution was exposed to 66 Torr ^{13}CO (1.6 mmol) and allowed to react for 1 h. The resulting clear yellow solution of THF-**2**-^{13}CO was degassed under vacuum and exposed to 450 Torr CO (~1 mmol) for 10 min at −78 °C and then warmed to 25 °C over the course of 3 h. The solvent and CO atmosphere were removed and an IR (C_6H_{12}) of the solid revealed a ~68:16:5:11 ratio of **6**:(**6**-^{13}CC):**6**-C^{13}C:**6**-$^{13}C_2$ in addition to **3**, indicative of significant exchange, but on a time scale less than that needed to produce a statistical mixture (88:6:6:~0.3).

9. (silox)$_3$Ta(CO)$_2$ (2-(CO)$_2$). a. Preparation. A 25-mL two-neck flask with a septum in one neck was charged with 30 mg of **2** (0.036 mmol) and attached to a 180° needle valve. By use of a graduated cylinder connected to a 180° needle valve, 10.0 mL of THF was measured out and vacuum transferred into the flask ([**2**] = 3.6×10^{-3} M). The solution was exposed at −78 °C to 1 atm CO from the manifold (18.4 mmol) and stirred for 1 h. Without degassing the solution, a 4-mL portion was withdrawn with a syringe cooled to −78 °C and the sample injected into the variable-temperature IR cell, which had previously been equilibrated to −63 °C. Two bands in the CO stretching region were observed at 1870 cm^{-1} (ν(^{13}CO) = 1832, calcd 1828 cm^{-1}) and 1840 cm^{-1} in an ~6:1 ratio. During the initial 15 min, the 1840-cm^{-1} band disappeared into the base line while the 1870-cm^{-1} stretch grew slightly. The 1870-cm^{-1} stretch remained contant over a 2-h period at −63 °C. While rapidly warming to 25 °C (~15 min), the band disappeared and a band at 2076 cm^{-1} formed (ketenylidene).

b. 2-(CO)$_2$ from THF-2-CO and Excess CO. A 25-mL two-neck flask with a septum in one neck was charged with 32 mg of (silox)$_3$Ta (0.039 mmol) and attached to a 180° needle valve. By use of a graduated cylinder connected to a 180° needle valve, 10.0 mL of THF was measured out and vacuum transferred into the flask at −78 °C ([**2**] = 3.9×10^{-3} M). The flask was back-filled with Ar and CO was then bubbled through the solution for 5 min. Without degassing the solution, a 4-mL portion was withdrawn with a syringe cooled to −78 °C and the sample injected into the variable-temperature IR cell, which had previously been equilibrated to −63 °C. Two bands in the CO stretching region were observed at 1870 and 1840 cm^{-1} in an ~2:7 ratio. Over time, the 1870-cm^{-1} stretch intensified at the expense of the 1840-cm^{-1} band. Both the disappearance of the 1840-cm^{-1} peak (2.9 half-lives, $k = 8.2$ (5) $\times$ 10^{-4} s^{-1}, $r^2 = 0.991$) and the appearance of the 1870-cm^{-1} band (2.0 half-lives, $k = 8.5$ (8) $\times$ 10^{-4} s^{-1}, $r^2 = 0.980$) followed first-order kinetics.

10. Intermediate Red Precipitate, [(silox)$_3$TaCO]$_n$ ([2-CO]$_n$). a. Synthesis. To a flask containing **2** (224 mg, contaminated with 8% oxo **3** by ^{1}H NMR) was distilled 25 mL of THF at −78 °C. While stirring, the solution was exposed to a manifold containing 450 Torr CO. A clear yellow solution was instantly formed. The bath was slowly warmed to −20 °C over 1.5 h, during which a red solid precipitated. The product was isolated by filtration at −20 °C and washed once with 10 mL of THF. The pale pink filtrate was collected in a preweighed flask and the volatiles were removed in vacuo. Reweighing the flask gave a difference of 20 mg (expected from the 8% impurity) and ^{1}H NMR of the residue showed only **3**. Therefore, complete CO bond cleavage to yield **3** has not yet occurred during formation of intermediate [**2**-CO]$_n$. On warming to 25 °C, the red solid slowly turned pale peach. An ^{1}H NMR showed a 1.1:1 ratio of **3** to **6**.

b. [2-CO]$_n$ and ^{13}CO to 5. A flask containing **2** (201 mg, 0.243 mmol) and 15 mL of hexane at −78 °C was exposed to ^{12}CO (90 Torr, 0.242 mmol, 1.00 equiv) from a calibrated gas bulb (50.1 mL). A deep red precipitate was immediately observed ([**2**-CO]$_n$). After stirring for 3 h, the solution was degassed with the Toepler pump and the gas collected in a 16-mL volume (14 Torr, 0.012 mmol), thus indicating an uptake of 0.95 equiv of CO (0.230 mmol/mmol of **2**). While still at −78 °C, the solution was exposed to 99 Torr 90% enriched ^{13}CO (1.6 mmol) and stirred for 3 h. On warming to 25 °C, the red precipitate was consumed to yield a clear blush solution. The solvent and carbon monoxide were removed under vacuum, 105 mg of **2** (0.127 mmol) added to the residue, and hexane distilled onto the mixture at −78 °C. An instantaneous reaction occurred to give brick-red dicarbide. The solution was warmed to 25 °C and stirred for 1 h. The dicarbide was isolated by filtration, washed twice with 5 mL of hexane, and dried in vacuo. An IR (Nujol) showed a 90:9:1 ratio of the isotopic dicarbide stretches at 711 (**5**), 698 (**5**-C^{13}C), and 687 (**5**-$^{13}C_2$) cm^{-1} consistent with less than 6% incorporation of ^{13}CO into intermediate [**2**-CO]$_n$.

c. [2-^{13}CO]$_n$ and CO to 5-$^{13}C_2$. The experiment in (b) was repeated except that [**2**-^{13}CO]$_n$ was generated from **2** and 90% ^{13}CO. The uptake of ^{13}CO was 0.88 mmol/mmol of **2**. As above, the red precipitate was allowed to warm under CO, and the resulting ketenylidenes were converted to dicarbide via the addition of **2**. An IR spectrum (Nujol) showed a 4:23:100 ratio of the isotopic dicarbide stretches at 711 (**5**), 698 (**5**-C^{13}C), and 687 (**5**-$^{13}C_2$) cm^{-1}. This is consistent with <5% incorporation of CO into intermediate [**2**-^{13}CO]$_n$ after correcting for the 90% enrichment of the ^{13}CO and the 0.88 uptake of ^{13}CO by **2** (predict 18:22:100 if no crossover; if the uptake of ^{13}CO was 1.0, then the ratio is 1:23:100).

d. Crossover of [2-CO]$_n$ and [2-^{13}CO]$_n$. To a two-neck flask charged with **2** (111 mg, 0.134 mmol) and capped with a septum was distilled 15 mL of hexanes at −78 °C. To another flask containing **2** (111 mg, 0.134 mmol) was also added 15 mL of hexanes at −78 °C. The two-neck flask was exposed to a manifold containing 102 Torr 90% ^{13}CO (1.6 mmol) and the other flask was opened to a manifold containing 102 Torr CO (1.6 mmol). Instantaneous reactions leading to red precipitates were observed in both cases. After 3 h the flasks were consecutively degassed. Under vigorous counterflow, the septum was replaced with a bent adapter and the second flask attached to the exposed end of the adapter. During this procedure, both flasks and the adapter were continuously swabbed with dry ice/acetone. A positive Ar atmosphere was maintained in the system. The contents of the flasks were mixed, allowed to stir at −78 °C for 30 min, and then warmed to 25 °C. After the opaque red solution became clear orange, the solvent was removed under vacuum. To the residue was added 109 mg of **2** (0.132 mmol). The mixture was allowed to react at 25 °C for 20 min in 20 mL of hexanes. Formation of dicarbide was observed. The brick-red solid was isolated by filtration, washed twice, and dried in vacuo. An IR (Nujol) spectrum showed a 53:9:39 ratio of the isotopic dicarbide stretches at 711 (**5**), 701 (**5**-C^{13}C), and 686 (**5**-$^{13}C_2$) cm^{-1}. If no crossover occurred, a 50:9:40 ratio would be observed for 90% ^{13}CO enrichment.

Physical Properties. 1. Extended Hückel Calculations. Parameters were taken from previous works.[82]

2. Magnetic Studies. a. General Procedure. Magnetic measurements were performed by the Faraday method[47,83-85] with $HgCo(SCN)_4$ as a calibrant (16.44×10^{-6} emu/g at 298 K). A detailed description of the instrument and the operational software is available.[85] A sealed bucket system, enabling sample loading in a drybox, was utilized for both **2** and **5**. Samples were transferred to the balance with an O-ring sealed container. Variable-field measurements (Honda–Owens plots)[47] were conducted to correct for ferromagnetic impurities. All measurements are corrected for the bucket force, shown to be temperature independent, and for sample diamagnetism by using standard Pascal constants.[86]

b. (silox)$_3$Ta (2). Measurements indicated the complex to be diamagnetic from 2 to 300 K, with χ_m(296 K) = -7.8×10^{-4} emu/mol, using the diamagnetic correction of -603.2×10^{-6} emu/mol.

c. [(silox)$_3$Ta]$_2$(μ-C$_2$) (5). The complex was examined over the temperature range 2 to 300 K, with the diamagnetic correction of -1218.3×10^{-6} emu/mol. A Honda–Owens plot of the susceptibility vs $1/H$ indicated the presence of a ferromagnetic impurity for which the data were adjusted. The fully corrected susceptibility data, χ_m^{corr}, and corresponding μ_{eff} are plotted vs temperature in Figure 4.

3. X-ray Crystal Structure of [(silox)$_3$Ta]$_2$(μ-C$_2$) (5). A dark red crystal, approximately 4 × 1.5 × 0.5 mm, was grown in a 5-mm NMR tube from THF. A 0.2 × 0.3 × 0.3 chip of this crystal was sealed under

(82) (a) Lauher, J. W.; Hoffmann, R. *J. Am. Chem. Soc.* **1976**, *98*, 1729–1742. (b) Hoffman, D. M.; Hoffmann, R.; Fiesel, C. R. *Ibid.* **1982**, *104*, 3858–3875.
(83) Kulick, J. D.; Scott, J. C. *J. Vac. Sci. Technol.* **1978**, *15*, 800–804.
(84) Morris, B. L.; Wold, A. *Rev. Sci. Instrum.* **1968**, *39*, 1937–1941.
(85) Richeson, D. S. Ph.D. Thesis, Cornell University, 1988.
(86) Hellwege, K.-H.; Hellwege, A. M., Eds. *Magnetic Properties of Coordination and Organometallic Transition Metal Compounds, Landolt-Bornstein Series*; Springer-Verlag: Berlin, 1981; Vol. 11.

N_2 in a thin-walled Lindemann capillary. Precise lattice constants for a triclinic cell, determined from a least-squares fit of 15 diffractometer-measured 2θ values at 25 °C, were a = 13.444 (7) Å, b = 13.028 (7) Å, c = 16.149 (8) Å, α = 69.13 (3)°, β = 87.57 (3)°, and γ = 120.03 (3)°. The cell volume was 2201 (2) Å^3 with a calculated density of 1.266 g/cm^3. The space group was determined to be $P\bar{1}$ (Z = 1) and the absorption coefficient (μ(Cu Kα)) was 56.07 cm^{-1}. All unique diffraction maxima ($h,\pm k,\pm l$) with $\theta \leq 110.0°$ were measured on a four-circle, computer-controlled diffractometer (Syntex $P2_1$) with a variable 1° ω scan using graphite-monochromated Cu Kα radiation (1.5418 Å). After correction for Lorenz, polarization, and background, 4054 (86.2%) of the merged and averaged unique data (4702) were judged observed ($|F_o| \geq 6\sigma(F_o)$).[87] Structure solution proceeded by using the SHELXTL PLUS system. The Ta was located via Patterson synthesis and the non-hydrogen light atoms were revealed with difficulty by successive Fourier syntheses. An inspection of difference maps following refinement of the initial model revealed disorder in each of the peripheral ^{t}Bu groups. After applying several models, one in which silox-1 (Si1, O1, etc.) contained two different sets of ^{t}Bu-group conformations related by a mirror plane proved to be best. Constraints were applied to the geometries of the ^{t}Bu fragments on each silox ligand such that chemically equivalent interatomic distances were constrained to equal the same least-squares variables (e.g., all d(SiC_{tert}) are equivalent; all d($C_{tert}C$) are equivalent; all d-($C_{tert}C_{tert}$) are equivalent, etc.). At the end of the isotropic refinement, the empirical absorption correction of Walker and Stuart was applied,[88] but this proved to have little effect (0.2%) on the final structure factors. Full-matrix, least-squares refinements (minimization of $\sum w(|F_o| - |F_c|)^2$, where w is based on counting statistics modified by an ignorance factor ($w^{-1} = \sigma^2(F) + 0.03F^2$)), with anisotropic Ta, Si, O, and carbide atoms, the remaining carbons included as isotropic and all hydrogens included at calculated positions (Riding model, fixed isotropic U), have converged to R = 9.56% and R_w = 10.05%.[89] A similar refinement using all unique data (4702, excluding zeros) resulted in an R of 10.5% and an R_w of 10.1%. The fractional coordinates and thermal parameters are listed in the supplemental material.

Acknowledgment. Primary support from the Air Force Office of Scientific Research (AFOSR-87-0103) and the National Science Foundation (CHE-8714146) are gratefully acknowledged as are contributions from Chevron Research Co., the Union Carbide Innovation Recognition Program, and Cornell University. We thank Profs. David B. Collum, Barry K. Carpenter, Francis J. DiSalvo, and Klaus H. Theopold for helpful discussions and John F. Mitchell for aid in the X-ray structural studies. We also thank Dr. Bruce Chase of Du Pont Central Research for conducting the Raman experiments. Support for the Cornell NMR facility from the NIH and NSF Instrumentation Programs is acknowledged.

Registry No. **1**, 102307-77-7; **2**, 104092-13-9; THF-**2**-CO, 123027-43-0; **2**-CO, 123027-44-1; **2**-$(CO)_2$, 123027-45-2; **3**, 123027-42-9; **4**, 102307-78-8; **5**, 104092-15-1; **5'**, 123027-40-7; **6**, 123027-41-8; **7**, 123051-54-7; Na(silox), 97733-16-9; CO, 630-08-0; (silox)H, 56889-90-8; PhC≡CPh, 501-65-5; ethylene, 74-85-1.

Supplementary Material Available: Honda-Owens plot of $[(silox)_3Ta]_2(\mu\text{-}C_2)$ (**5**), Curie plot of $(silox)_3$(THF)TaCO (THF-**2**-CO), tables of crystal data encompassing data collection and solution and refinement, figures showing the disorder model, tables of atomic coordinates and isotropic temperature factors, anisotropic temperature factors of core atoms, hydrogen atom coordinates, bond lengths, and bond angles for **5** (13 pages); listing of observed and calculated structure factors (17 pages). Ordering information is given on any current masthead page.

(87) Cromer, D. T.; Mann, J. B. *Acta Crystalogr., Sect. A* **1968**, *A24*, 321-324.

(88) Walker, N.; Stuart, D. *Acta Crystallogr., Sect. A* **1983**, *A39*, 158-166.

(89) $R = \sum||F_o| - |F_c||/(\sum|F_o|)$; $R_w = \{\sum w(|F_o| - |F_c|)^2/\sum w(|F_o|)^2\}^{1/2}$.

Vibrational Characterization of Multiply Metal-Metal Bonded Osmium, Molybdenum, and Rhenium Porphyrin Dimers

C. Drew Tait,[1a] James M. Garner,[1b] James P. Collman,*[,1b] Alfred P. Sattelberger,*[,1a] and William H. Woodruff*[,1a]

Contribution from the Inorganic and Structural Chemistry Group (INC-4), Los Alamos National Laboratory, Los Alamos, New Mexico 87545, and the Department of Chemistry, Stanford University, Stanford, California 94305. *Received May 18, 1989*

Abstract: The resonance Raman (RR) scattering and infrared (IR) absorption spectra of $\{[M(OEP)]_2\}^{n+}$ complexes [OEP = 2,3,7,8,12,13,17,18-octaethylporphyrin dianion; M = Os (n = 0-2), Re (n = 0-2), and Mo (n = 0)] are reported. Resonance Raman studies reveal the Os-Os stretch to increase in frequency upon oxidation [233 cm^{-1} (n = 0), 254 cm^{-1} (n = 1), and 266 cm^{-1} (n = 2)], consistent with the removal of electrons from π^* metal-metal antibonding orbitals. The Mo-Mo stretch was also observed spectroscopically, producing a RR peak at 341 cm^{-1}, while the Re-Re stretch in $\{[Re(OEP)]_2\}^{1+}$ was observed at 290 cm^{-1}. The corresponding metal-metal bond distances estimated from these stretching frequencies are 2.39, 2.31, and 2.27 Å for the osmium oxidation series, 2.23 Å for the molybdenum dimer, and 2.20 Å for the rhenium dimer. The porphyrin-centered vibrational modes (both RR and IR active) for the three osmium complexes are essentially independent of oxidation state, consistent with oxidation of metal-metal antibonding electrons. Little π back-bonding between the metal and porphyrin macrocycle is suggested from porphyrin RR indicator modes, which are sensitive to π electron density. Moreover, the porphyrin core size (center to nitrogen distance) is estimated from core size marker vibrations to be ca. 2.04 Å for all of the complexes studied. Finally, no vibrational evidence for ground-state intradimer coupling between the π orbitals of the porphyrin rings is found.

Detailed spectroscopic and structural investigations of binuclear transition-metal complexes containing unbridged metal-metal multiple bonds are often compromised by the failure of ancillary ligands to remain substitutionally inert when the dimers are oxidized or reduced.[2-4] Ligand lability in the redox partners fre-

(1) (a) Los Alamos National Laboratory. (b) Stanford University.

(2) Cotton, F. A.; Walton, R. A. *Multiple Bonds between Metal Atoms*; Wiley: New York, 1982.

0002-7863/89/1511-9072$01.50/0